Summary of HTGR Benchmark Data from the High Temperature Lattice Test Reactor

D. F. Newman

October 1989

❀ Battelle

DO NOT MICROFILM COVER

DISCLAIMER

DISCLAIMER

Portions of this document may be illegible in electronic image products. Images are produced from the best available original document.

The following pages are an exact representation of what is in the original document folder.

SUMMARY OF HTGR BENCHMARK DATA
FROM THE HIGH TEMPERATURE
LATTICE TEST REACTOR

D. F. Newman

October 1989

MASTER

THIS PAGE

WAS INTENTIONALLY

LEFT BLANK

SUMMARY

The High Temperature Lattice Test Reactor (HTLTR) was a unique critical facility specifically built and operated to measure variations in neutronic characteristics of high temperature gas cooled reactor (HTGR) lattices at temperatures up to 1000°C. The Los Alamos National Laboratory commissioned Pacific Northwest Laboratory (PNL) to prepare this summary reference report on the HTLTR benchmark data and its associated documentation. Extensive efforts were applied by PNL since 1965, throughout the experimental and analytic phases of the benchmark data generation, to provide validation and verification of the results. In the initial stages of the program, the principle of the measurement of k_∞ using the unpoisoned technique (developed by R. E. Heineman of PNL) was subjected to extensive peer review within PNL and the General Atomic Company. A number of experiments were conducted at PNL in the Physical Constants Testing Reactor (PCTR) using both the unpoisoned technique and the well-established null reactivity technique that substantiated the equivalence of the measurements by direct comparison. The methods used and the experimental results were published in peer-reviewed journals: Nuclear Science and Engineering and Nuclear Technology as well as being presented at National meetings of the American Nuclear Society and published in Transactions of the American Nuclear Society. Records of all data from fuel fabrication, the reactor experiments, and the analytical results were compiled and maintained to meet applicable quality assurance standards in place at PNL. Sensitivity of comparisons between measured and calculated $k_\infty(T)$ data for various HTGR lattices to changes in neutron cross section data, graphite scattering kernel models, and fuel block loading variations, were analyzed by PNL for the Electric Power Research Institute. The results of this review and correlation of calculated and measured results was published in the peer-reviewed journal, Nuclear Technology. As a part of this effort, the fuel rod composition in the dilute $^{233}UO_2$-ThO_2 HTGR central cell (HTLTR Lattice #3) was sampled and analyzed by mass spectrometry. Values of k_∞ calculated for that lattice were about 5% higher than those measured. Trace quantities of sodium chloride were found in the fuel rod that were equivalent to 22 atom parts-per-million of natural boron.

Calculations that included this impurity concentration in the fuel were in good agreement with the measured value at room temperature.

External peer reviewers of the HTLTR benchmark data and analyses included: R. C. Dahlberg, J. R. Brown, D. R. Mathews, and K. R. Schultz (General Atomic); G. L. Ragan (ORNL); Odelli Ozer (EPRI). The measured $k_\infty(T)$ data, summarized in this report, provides a verifiable basis for validating temperature coefficients of reactivity for HTGR lattices, even though they predate NQA-1 requirements.

CONTENTS

TABLES

INTRODUCTION

The reactivity behavior of a high-temperature gas-cooled reactor (HTGR), which uses helium gas as coolant, is insensitive to changes in coolant density. As a result, reactivity control of graphite-moderated HTGRs is simplified from that of light-water reactors (LWRs) or heavy-water reactors (HWRs), where the moderator is also the coolant and can undergo a phase change. In addition, an HTGR has a large thermal capacity in the core that can absorb excess heat without rapid changes in fuel or moderator temperatures. However, a negative temperature coefficient of reactivity both for the fuel kernels (prompt) and for the entire lattice (isothermal) is necessary at all stages of operation to provide a stabilizing feedback effect to cope with reactivity insertions and transients. All anticipated reactivity control functions in an HTGR, such as shim, burnup, and power distribution control, are performed by control rods that can be moved vertically in channels provided in some of the fuel block stacks.

The prismatic HTGR fuel block was developed by General Atomic in the late 1960s to eliminate some problems encountered with full-length tubular fuel elements employed in the early HTGR prototype, Peach Bottom-1. Prismatic fuel blocks were used in the 330 MWe Ft. St. Vrain (FSV) HTGR that was operated by Public Service Co. of Colorado in the 1970s and early 1980s. To support the development and licensing efforts on FSV, the U.S. Atomic Energy Commission funded the design, construction, and operation of the High-Temperature Lattice Reactor (HTLTR) at the Pacific Northwest Laboratory. The HTLTR was the only facility capable of measuring the isothermal reactivity behavior of HTGR cores up to 1300 K with high precision. PNL conducted experiments with five different HTGR cores in the HTLTR between 1968 and 1971. The chronology of these HTLTR operations is shown in Figure 1. These experiments included measurements of the temperature-dependent neutron multiplication factor, $k_\infty(T)$, temperature coefficients of reactivity, thorium Doppler coefficient, and other integral neutronic data. Results of the HTLTR experiments provided the basis for validation of GA and PNL calculational methods and cross-section data used for HTGR neutronic design and safety analysis and to quantify the bias in calculated predictions of temperature coefficients of reactivity in HTGR lattices.

1
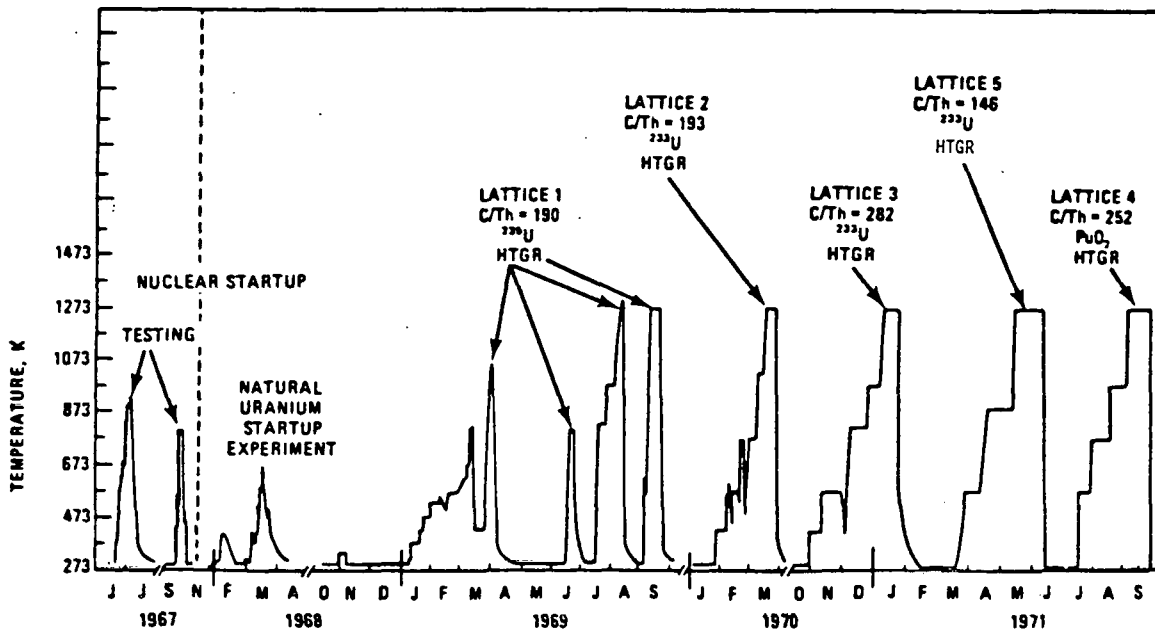
FIGURE 1. HTLTR Experimental History

The FSV HTGR used highly enriched uranium and thorium fuel. The thorium content provided the main negative contribution to the prompt and isothermal temperature coefficients of reactivity through the Doppler effect on the neutron capture resonances of thorium. At the beginning-of-life of an HTGR core, other significant contributions to the temperature coefficient of reactivity are due to effects from ^{235}U, lumped burnable poison, inserted control rods, and neutron leakage. Three of the HTGR cores operated in the HTLTR contained ^{233}U and thorium. These compositions were selected to determine variations in the temperature coefficients of reactivity in an HTGR due to buildup of ^{233}U in-situ and recycle operations.[1] Predicted values of the temperature coefficient of reactivity for fresh ^{233}U recycle HTGR lattice are negative at temperatures below 1600 K, as shown in Figure 2, due to the Doppler effect on thorium resonance neutron capture.
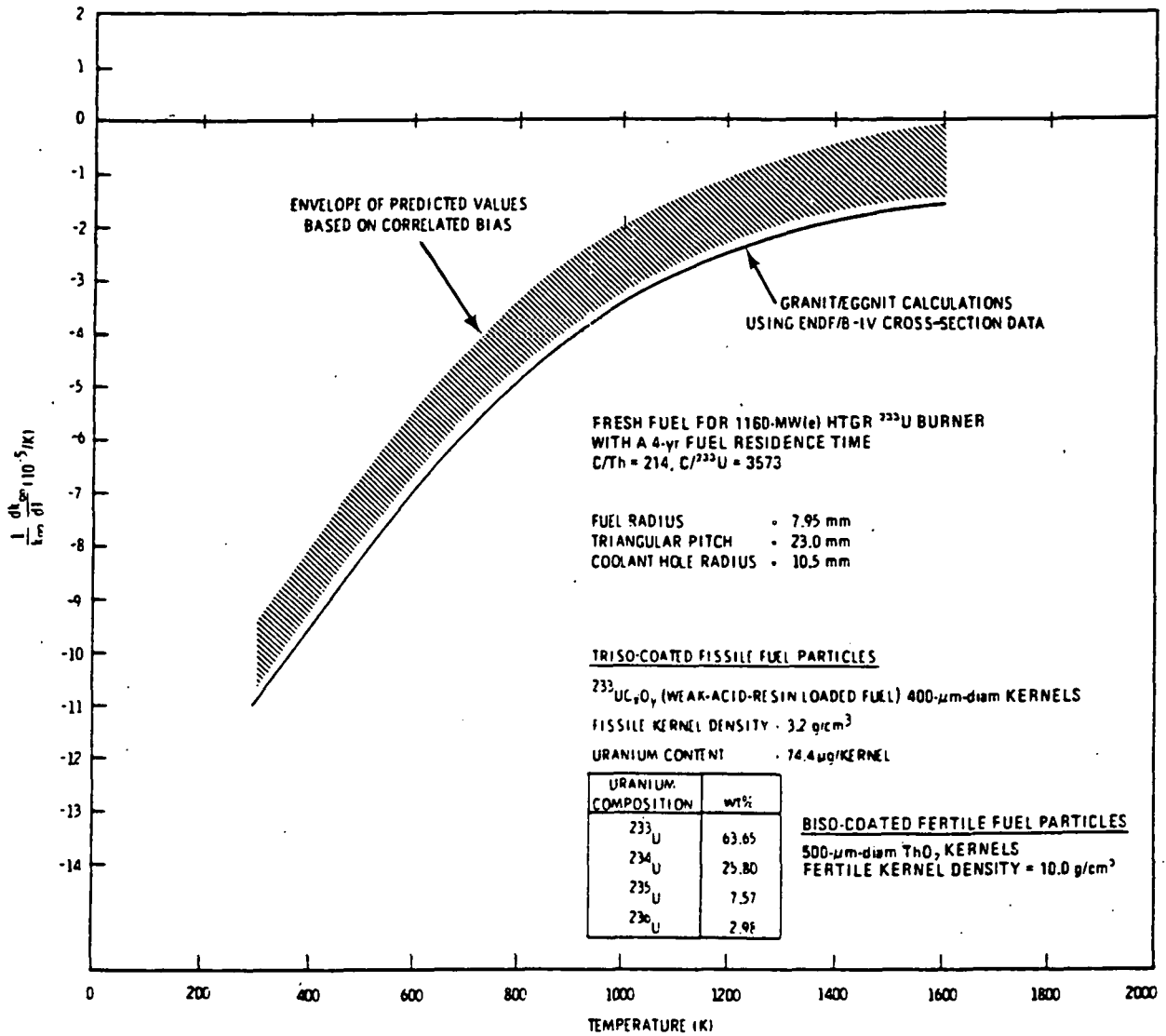
FIGURE 2. Temperature Coefficient of Reactivity Calculated for a Fresh
HTGR ^{233}U Burner Lattice Using ENDF/B-IV Data

DESCRIPTION OF THE HTLTR

The design of the HTLTR facility was drawn from the experience of a number of predecessors in the field of heated critical assemblies, HERO[2] in Great Britain, CESAR[3] in France, and HOT BOX[4] in the United States. Some of its features were unique, however. In particular, the capability to operate at an ambient temperature of 1000°C (1273 K, 1832°F), for extended periods of time (several weeks) and to make precise measurements of reactivity worth of sample lattice materials while at temperature was not equaled anywhere.

The HTLTR and its supporting facilities are shown in Figure 3. The reactor consisted of a 10-ft cube of graphite enclosed in a carbon steel shell oven which was thermally insulated and gas tight.
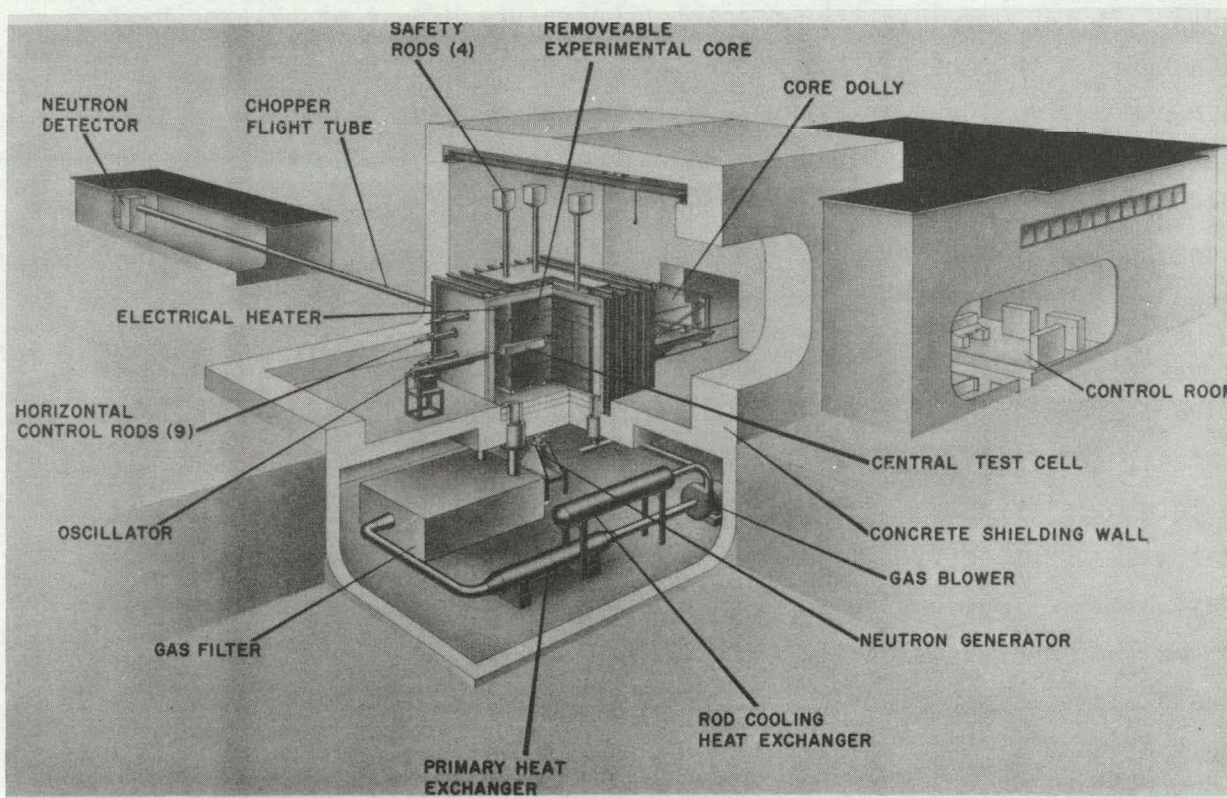
FIGURE 3. Schematic Illustration of HTLTR and Supporting Facilities

The reactor was made up of cored, nuclear grade graphite bars which were stacked, keyed, and doweled together to form a solid unit. The 5-ft-square by 10-ft-long central section was removable to permit loading of different test assemblies. The central test cell of an experimental core could thereby be provided with a flux environment characteristic of its own kind of cells in a critical array. Driver fuel and control rods were located in symmetric positions surrounding the test section. The reactor, rated at 2 kW for nuclear operation, was heated electrically and operated with average temperatures of the graphite cube up to 1000°C. A maximum of 384 kW of electrical power could be applied to heat the reactor, using 24 graphite heater bars that extended through the 10-ft length of the graphite stack. A thermally insulated, gas-tight, steel shell around the reactor made the assembly essentially a furnace. Nitrogen gas was used to provide an inert atmosphere to inhibit oxidation of the carbon moderator. The nitrogen also served as a coolant to rapidly lower the reactor temperature by use of a large heat exchanger in the gas system. A photograph of the HTLTR with the front shell door removed is shown in Figure 4. The front face of the graphite stack is shown with a simulated HTGR test core in place. A viewing port was provided near the front face of the HTLTR shell which permitted observation of sample changing in the reactor at all temperatures. A photograph taken through this viewer at 1000°C is shown in Figure 5.

Enriched uranium driver fuel was used to make the HTLTR critical. The driver assemblies consisted of UO_2 (5 wt% ^{235}U) ceramic pellets, 1.06 in. in diameter and 1/2 in. thick, loaded into graphite tubes 1.6-in. o.d. The fuel pellets were arranged in the fuel assemblies such that each 1-in. length of fuel was separated by 2 in. of graphite. Three fuel element lengths were available: 6, 10, and 60 in. The 60-in.-long assemblies were the main driver fuel and were located in a ring around the test core. The shorter length elements were located on the ends of the test core and served to level the spatial distribution of the neutron flux in the longitudinal direction.

Fine control of the neutron multiplication in the HTLTR was maintained by eight shutter-type control rods whose active length was 90 in. The control rods were located symmetrically about the axis at a radial distance of 38 in. and ran parallel to the axis of the reactor. A ninth rod, having
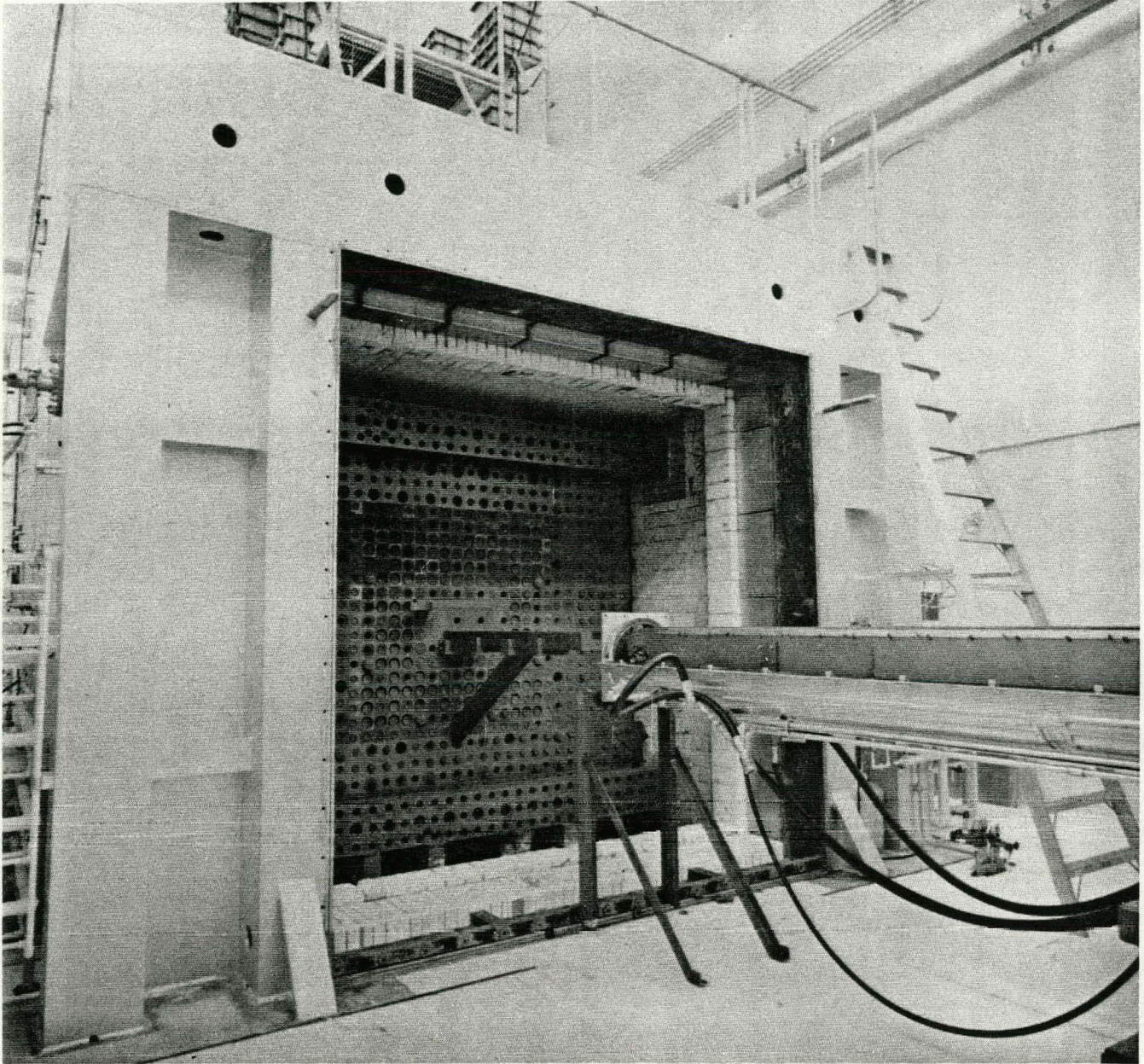
FIGURE 4. Front Face of HTLTR with Shell Door Removed

only a small fraction of the strength of the primary control rod, was
provided to obtain precise measurements of small reactivity changes. This
rod was located 56 in. from the axis and had an active length of only 30 in.
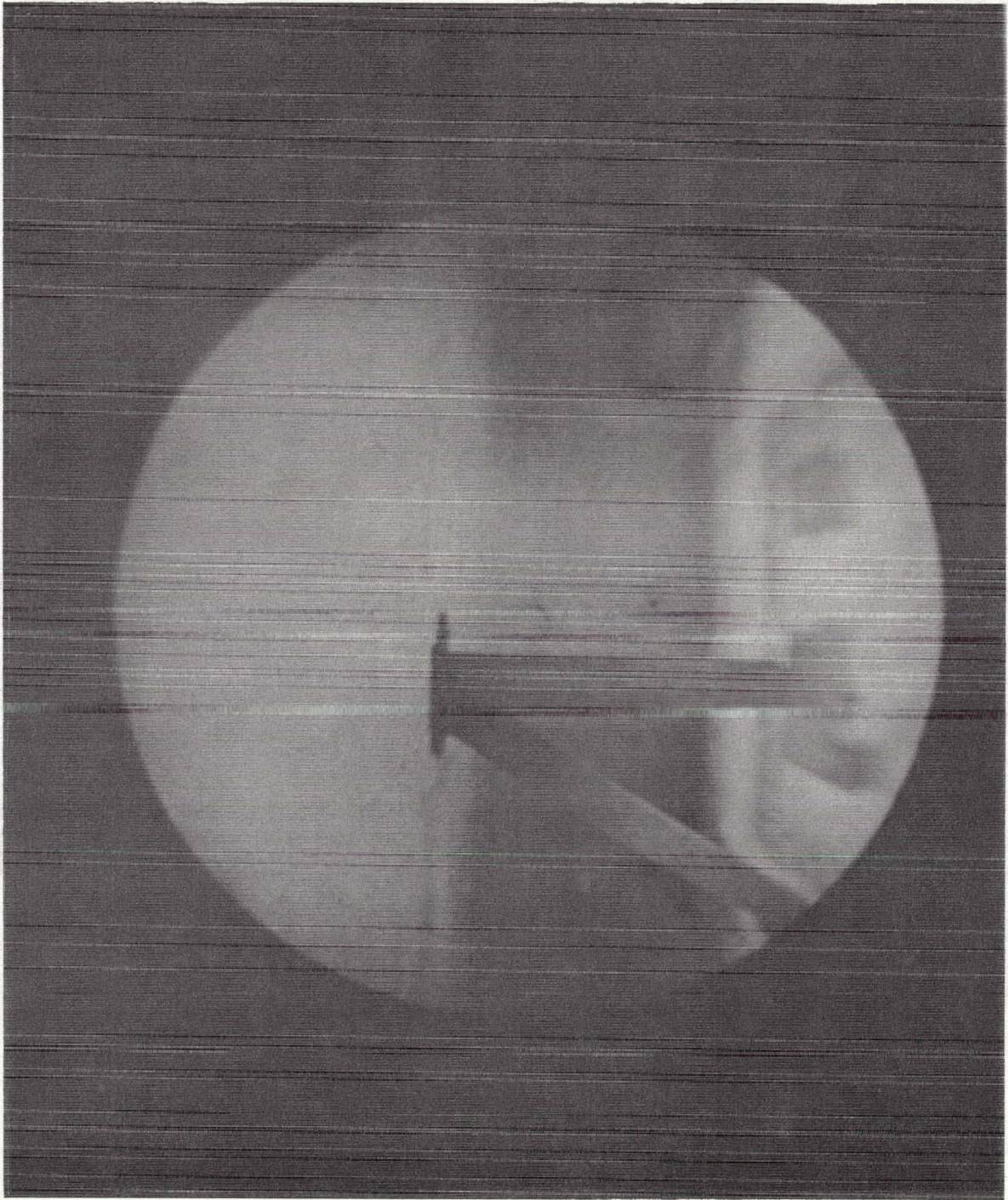
FIGURE 5. HTLTR Graphite Stack at 1000°C

Each control rod, illustrated in Figure 6, consisted of two concentric tubes made up alternately of 6-in.-long graphite cylinders and cylinders of UO_2 dispersed in graphite (3 g/cm^3 UO_2, 16 wt% ^{235}U). The outer tube, 2.1-in. o.d. and 1.44-in. i.d., was held stationary with respect to the reactor. The inner tube, 1.37-in. o.d. and 0.75-in. i.d., was assembled on a 1/2-in.-dia thoria-dispersed nickel (TD nickel) rod which is connected to a driving mechanism located at the rear of the reactor and outside the reactor shell. A change in the reactivity of the reactor was obtained by changing the mutual neutron shielding between the fuel sections of the inner and outer control tubes. In the closed position (position of maximum shielding and least reactivity) the UO_2-graphite sections of the inner tube appeared under the UO_2-graphite sections of the outer tube. For the open position (position of least shielding and maximum reactivity) the UO_2-graphite sections of the inner tube appeared under the graphite sections of the outer tube. A full change of reactivity was thus obtained with only a 6-in. movement of the inner control tube.
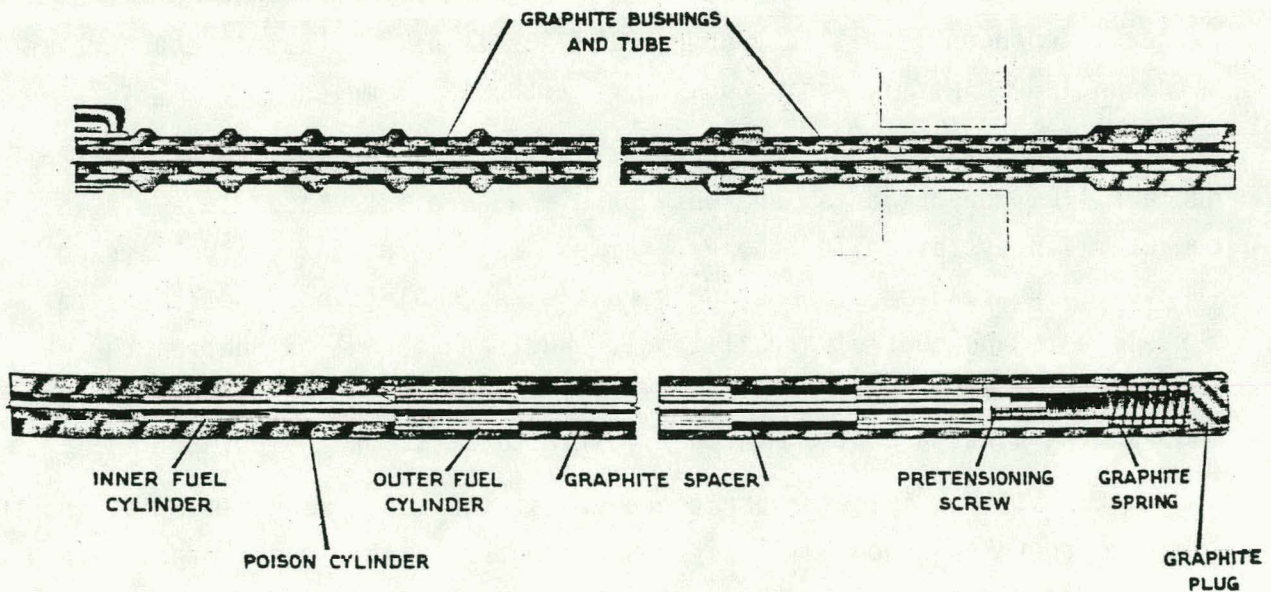
FIGURE 6. HTLTR Control Rods

9

A system of four vertical safety blades ensured reactor shutdown capability at all times. Each safety blade was 7 in. wide, about 138 in. long, and 1/2 in. thick. A nickel matrix containing a dispersion of 4 wt% Gd_2O_3 and 4 wt% Eu_2O_3 comprising the neutron absorber, in pieces 6 in. square and 1/16 in. thick, made up an active length of 120 in. These nuclear poison squares were mounted in a ladder frame made up of 1/2-in.-dia. TD-nickel rods. Each poison plate was covered on each side with a 0.030-in.-thick TD-nickel sheet which served as a radiant energy shield. The four safety blades moved in vertical rectangular slots located in the reactor moderator.

Two sample changers were available for replacement and repositioning of samples in the reactor at high temperatures with the nitrogen atmosphere in the reactor protected. One of the sample changers was for moving small samples into the reactor; the other sample changer, which is shown in Figure 7, was for heavier samples such as a central test cell. This heavy-duty sample changer had an electrically heated oven in it for preheating the samples before insertion in the reactor. Preheating enabled temperature transients during sample changes to be minimized in the HTLTR. Each sample changer could be sealed from the reactor atmosphere and pumped down and purged independently with nitrogen. The shells of both sample changers were water cooled to permit rapid cooling of withdrawn samples.

All the sensors and transducers essential for reactor process control, nuclear flux measurements, and data handling were interfaced to a single computerized system called the Programmed Measurement and Control System (PMACS). The reactor systems and hardware were maintained under computer surveillance and control at all times. Nuclear control of the reactor was not a closed loop, however, since reactivity additions to the reactor must be made under operator control through instructions to the computer.

After sitting idle for about ten years, the HTLTR was dismantled and the large concrete-shielded cell that contained the reactor was converted into a radiation dosimetry calibration facility.
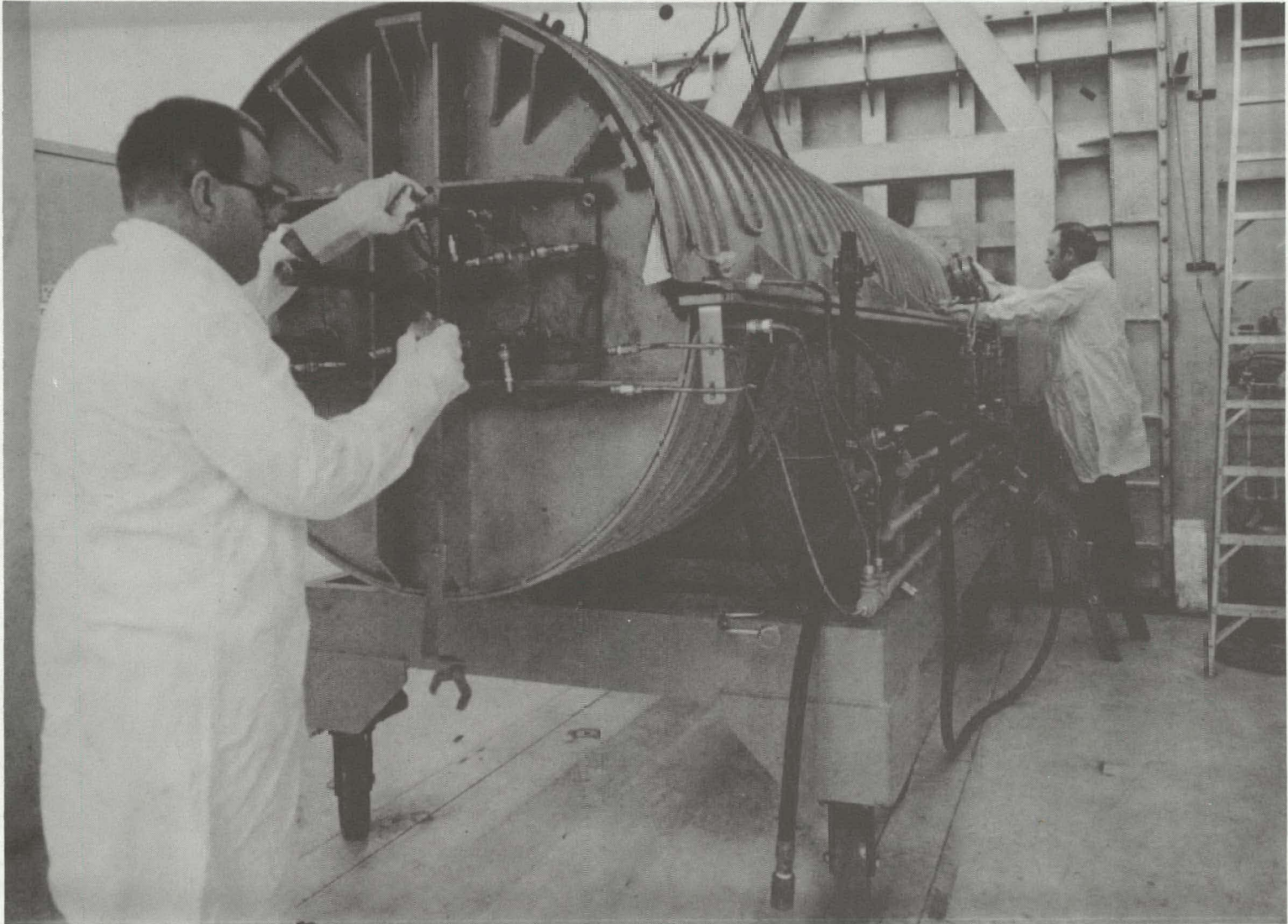
FIGURE 7. HTLTR Remote Sample Changer with Preheating Capabilities

HTGR BENCHMARK DATA

The HTGR cores tested in the HTLTR used fuel blocks with simplified geometry; no coolant channels were provided. Each HTLTR lattice fuel block was 3.75-in. square. Four of the five HTLTR lattices used 0.47-in. diameter fuel rods on a 0.75-in. pitch as illustrated in Figure 8. The fifth lattice used 0.786-in. diameter fuel rods on a 1.875-in. square pitch. The fissile fuel particles used in the fuel rods were coated with pyrolytic carbon, as shown in Figure 9.

All of the HTGR fuel blocks used in the HTLTR were fabricated at PNL. Fissile fuel microspheres enclosed in a pyrocarbon coating were specially prepared at Oak Ridge National Laboratory (ORNL) for each of the five test cores. The amount of fissile fuel in these coated microspheres was chemically analyzed by ORNL to an estimated accuracy of 1%. Therefore, although the total weight of coated microspheres in each block is accurately known, the amount of fissile material in each block has a 1% uncertainty. A much smaller uncertainty exists for the total amount of thorium and graphite particles loaded in the fuel channels of each block. The thoria particles were uncoated and consisted of irregular shapes of various sizes. The graphite particles were prepared by collecting powder milled from nuclear-grade graphite blocks at PNL. The loading procedure described in reference 21 was used to achieve a homogeneous fuel distribution throughout each fuel channel. Loaded blocks were X-rayed as an overall check of uniformity.

A sufficient number of blocks (about 150) of each core composition were loaded in the center of the HTLTR to establish the equilibrium neutron spectrum characteristic of a critical assembly of each core being tested. Values of the neutron multiplication factor, k_∞, were measured at several temperatures for each HTGR core being tested.

Using the composition and geometry known for each of the test cores, values of k_∞ were calculated for each core as a function of temperature. The GRANIT[5] and EGGNIT[6] codes were used for these calculations using ENDF/B-IV neutron cross-section data. These codes are capable of handling multiregion and granular composite geometries encountered in HTGR fuel assemblies. The GRANIT code calculates the spatially dependent
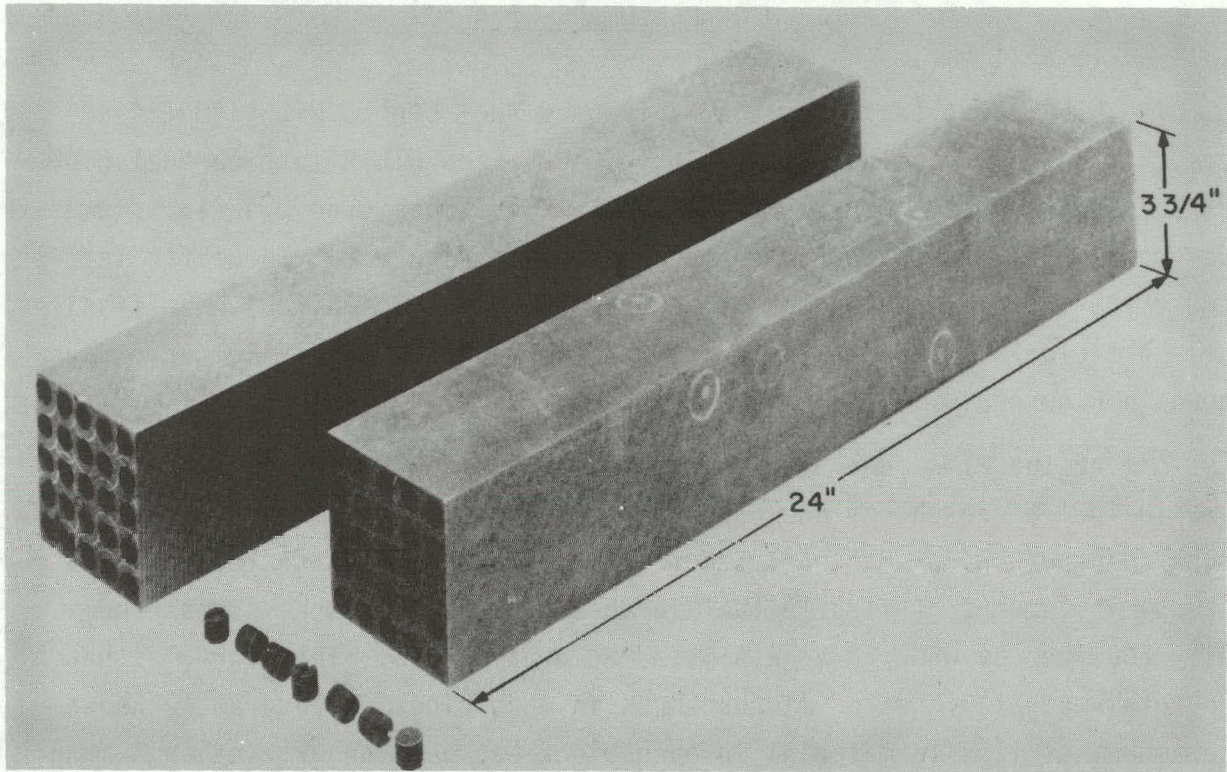
FIGURE 8. Typical Fuel Block for HTGR Experiments in the HTLTR

thermal-neutron spectra, reaction rates, and spectrum-averaged neutronic parameters for a unit lattice cell of an HTGR using 48 energy groups below 3.06 eV. The EGGNIT code calculates resonance self-shielding, neutron spectra, and reaction rates for the lattice cell in 60 energy groups from 10 MeV to 3.06 eV. These neutron spectra calculations, using the B_1 approximation, are coupled using the critical equation

$$k_{eff} = 1 = \frac{k_{\infty}\left[1 + (1-p)\, L^2 B^2\right]}{\left(1 + \tau B^2\right)\left(1 + L^2 B^2\right)} \quad (1)$$

14
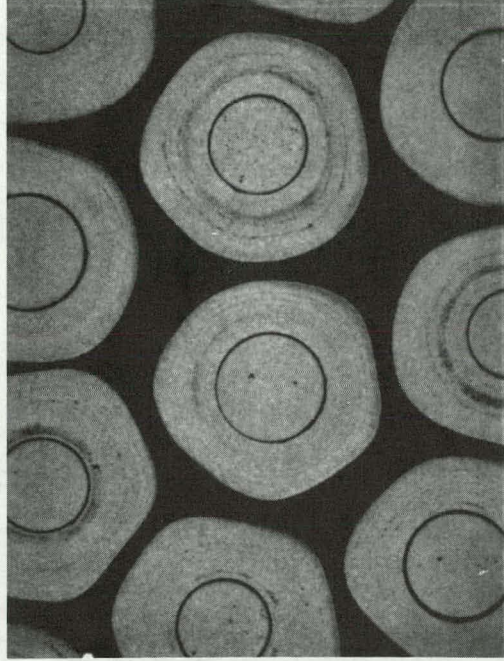
FIGURE 9. Pyrocarbon Coated PuO_2 Microspheres for
ThO_2-PuO_2 HTGR Lattice

where

$$k_\infty = \frac{\eta_1 f_1 \left(1-p\right)\left(1 + L^2 B^2\right) + \eta_2 f_2 p}{1 + (1-p) L^2 B^2} \quad , \tag{2}$$

$$\tau = \frac{D_1}{\Sigma_{1\to 2} + \Sigma a_1} \quad , \quad \eta_1 f_1 = \left(\frac{\nu\Sigma_f}{\Sigma a}\right)_1 \quad , \quad \eta_2 f_2 = \left(\frac{\nu\Sigma_f}{\Sigma a}\right)_2 \quad ,$$

$$p = \frac{\Sigma_{1\to 2}}{\Sigma_{1\to 2} + \Sigma a_1} \quad , \quad L^2 = \frac{D_2}{\Sigma a_2}$$

and B^2 is the material buckling which satisfies both equations (1) and (2).

Compositions for the $^{235}UC_2$-ThO_2 HTGR lattice are listed in Table 1; the C/Th atom ratio is 190 and the C/^{235}U atom ratio is 5710.[7] The C/Th atom ratio is similar to that of FSV and the highly enriched ^{235}U particulate fuel

15

TABLE 1. Composition of $^{235}UC_2$-ThO_2 HTGR Lattice

	Concentration (atoms/b-cm)				
Nuclide	UC_2 Particles	ThO_2 Particles	Fuel Rod Region	Moderator Region	Homogenized Cell Average
^{234}U	1.39-04	--	2.42-07	--	7.45-08
^{235}U	2.27-02	--	3.94-05	--	1.22-05
^{236}U	7.30-05	--	1.27-07	--	3.91-08
^{238}U	1.30-03	--	2.26-06	--	6.97-07
^{232}Th	--	2.28-02	1.18-03	--	3.65-04
Oxygen	--	4.56-02	2.37-03	--	7.30-04
Nitrogen[a]	--	--	2.66-05	1.40-05	1.79-05
Carbon	4.84-02	--	4.63-02	7.98-02	6.95-02

(a) At 296 K. For other temperatures $N_n(T) = N_n(296) \frac{296}{T\ (K)}$

C/Th = 190, C/^{235}U = 5710. (HTLTR Lattice 1)
Fuel rod radius = 0.5969 cm.
Square lattice pitch = 1.905 cm.

Distribution of ThO_2 Particle Sizes			Distribution of UC_2 Particle Sizes	
Particle Diameter Range (μm)	Average Particle Diameter (cm)	Weight Percent	Average Particle Diameter (cm)	Weight Percent
0- 44	0.0022	49.4	0.0270	19
44- 74	0.0059	16.4	0.0290	26
74-105	0.00895	19.4	0.0320	20
105-149	0.0127	11.1	0.0340	17
149-210	0.01795	3.7	0.0370	10
			0.0390	8

is of the same type used in FSV. Results of comparisons of experimental and calculated k_∞ values for the $^{235}UC_2$-ThO_2 HTGR lattice are shown in Figure 10 and listed in Table 2.[8]

Compositions for the three $^{233}UO_2$-ThO_2 HTGR lattices[9,10,11] are listed in Tables 3, 4, and 5. The C/Th atom ratio for these lattices are 282, 193, and 146. The $^{233}UO_2$-ThO_2 particles are about 300μ diameter and have a Th/U atom ratio of 3. Additional particles of pure ThO_2 were added to

$^{235}UC_2$ - ThO_2 HTGR LATTICE
C/Th = 190
C/^{235}U = 5710

CURRENT GRANIT/EGGNIT CALCULATIONS
WITH ENDF/B-IV CROSS SECTION DATA

CORRELATED LEAST SQUARES FIT

PREVIOUSLY REPORTED
GRANIT/EGGNIT CALCULATIONS
USING BATTELLE MASTER LIBRARY
CROSS SECTION DATA
C.R. RICHEY AND I.J. OAKES NUC. SCI. ENG., 47, 54, (1972)
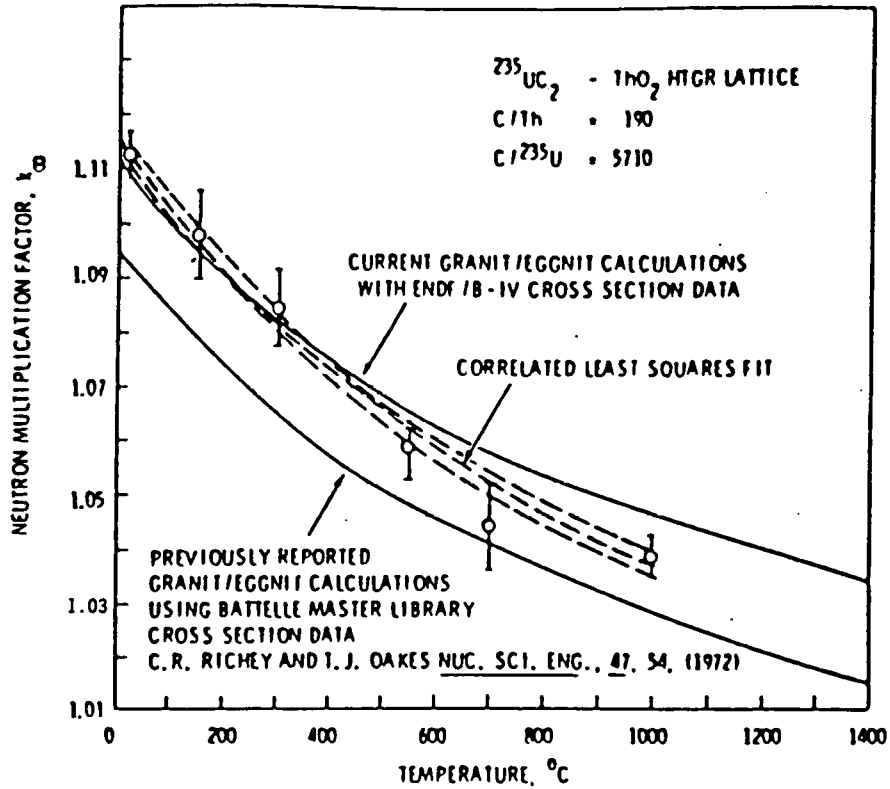
FIGURE 10. Comparison of Calculated and Measured Neutron Multiplication Factors as a Function of Temperature

TABLE 2. Experimental and Calculated Parameters for a $^{235}UC_2$-ThO_2 Lattice

(HTLTR Lattice 1); GRANIT/EGGNIT Calculations[8] Used ENDF/B-IV Cross-Section Data

| Temperature (K) | Experimental Values | | Calculated Values |
	Measured k_∞	Best Theory Least-Squares-Fit to Measured Data k_∞	All Data from ENDF/B-IV k_∞
293	1.1126±0.004	1.1124	1.1093
423	1.0979±0.008	1.0965	1.0950
573	1.0845±0.007	1.0821	1.0823
823	1.0591±0.006	1.0628	1.0659
973	1.0444±0.008	1.0537	1.0585
1273	1.0388±0.004	1.0387	1.0468

17

TABLE 3. Composition of $^{233}UO_2$-ThO_2 Dilute HTGR Lattice

	Concentration (atom/b-cm)				
Nuclide	UO_2-ThO_2 Particles	ThO_2 Particles	Fuel Rod Region	Moderator Region	Homogenized Cell Average
^{233}U	5.57-03	--	1.63-05	--	5.04-06
^{234}U	5.93-05	--	1.74-07	--	5.36-08
^{235}U	5.50-06	--	1.61-08	--	4.97-09
^{236}U	3.39-07	--	9.93-10	--	3.06-10
^{238}U	8.00-05	--	2.35-07	--	7.24-08
^{232}Th	1.71-02	2.28-02	8.11-04	--	2.50-04
Oxygen	4.56-02	4.56-02	1.65-03	--	5.10-04
Nitrogen[a]	--	--	2.69-05	1.47-05	1.85-05
Carbon	--	--	4.88-02	8.01-02	7.04-02
Boron	--	--	1.13-06	--	3.49-07

(a) At 296 K. For other temperatures, $N_n(T) = N_n(296) \frac{296}{T (K)}$.
C/Th = 282, C/^{233}U = 13,990. (HTLTR Lattice 3)
Fuel rod radius = 5.969 mm.
Square lattice pitch = 19.05 mm.
UO_2O-ThO_2 particle diameter = 0.322 mm.

Distribution of ThO_2 Particle Sizes		
Particle Diameter Range (μm)	Average Particle Diameter (mm)	Weight Percent
0- 44	0.022	15.0
44- 74	0.059	10.5
74-105	0.0895	11.5
105-149	0.127	15.0
149-210	0.1795	22.0
>210	0.250	26.0

TABLE 4. Composition of $^{233}UO_2$-ThO_2 HTGR Lattice

Nuclide	Concentration (atom/b-cm)				
	UO_2-ThO_2 Particles	ThO_2 Particles	Fuel Rod Region	Moderator Region	Homogenized Cell Average
^{233}U	5.57-03	--	2.19-05	--	6.76-06
^{234}U	5.97-05	--	2.35-07	--	7.25-08
^{235}U	4.83-06	--	1.90-08	--	5.86-09
^{236}U	5.07-07	--	2.00-09	--	6.17-10
^{238}U	7.50-05	--	2.95-07	--	9.10-08
^{232}Th	1.71-02	2.28-02	1.19-03	--	3.67-04
Oxygen	4.57-02	4.56-02	2.43-03	--	7.49-04
Nitrogen[a]	--	--	2.63-05	1.44-05	1.80-05
Carbon	--	--	4.84-02	8.09-02	7.09-02

(a) At 296 K. For other temperatures, $N_n(T) = N_n(296) \frac{296}{T~(K)}$.
C/Th = 193, C/^{233}U = 10,470. (HTLTR Lattice 2)
Fuel rod radius = 5.969 mm.
Square lattice pitch = 19.05 mm.
UO_2-ThO_2 particle diameter = 0.280 mm.

Distribution of ThO_2 Particle Sizes		
Particle Diameter Range (μm)	Average Particle Diameter (mm)	Weight Percent
0- 44	0.022	49.4
44- 74	0.059	16.4
74-105	0.0895	19.4
105-149	0.127	11.1
149-210	0.1795	3.7

the fuel rods to achieve the desired compositions. Results of comparisons of experimental and calculated k_∞ values for the $^{233}UO_2$-ThO_2 HTGR lattices are shown in Figures 11, 12, and 13; numerical values are listed in Tables 6, 7, and 8.

TABLE 5. Composition of $^{233}UO_2$-ThO_2 HTGR Lattice (2/3 larger fuel rod)

	Concentration (atom/b-cm)				
Nuclide	UO_2-ThO_2 Particles	ThO_2 Particles	Fuel Rod Region	Moderator Region	Homogenized Cell Average
^{233}U	5.74-03	--	5.69-05	--	7.85-06
^{234}U	6.13-05	--	6.08-07	--	8.39-08
^{235}U	5.37-06	--	5.32-08	--	7.34-09
^{236}U	4.04-07	--	4.00-09	--	5.52-10
^{238}U	8.15-05	--	8.08-07	--	1.12-07
^{232}Th	1.69-02	2.25-02	3.70-03	--	5.10-04
Oxygen	4.56-02	4.50-02	7.50-03	--	1.04-03
Nitrogen[a]	--	--	2.49-05	1.48-05	1.61-05
Carbon	--	--	3.87-02	8.00-02	7.43-02

(a) At 296 K. For other temperatures, $N_n(T) = N_n(296) \frac{296}{T (K)}$.

C/Th = 146, $C/^{233}U$ = 9460. (HTLTR Lattice 5)
Fuel rod radius = 9.982 mm.
Square lattice pitch = 47.63 mm.
UO_2-ThO_2 particle diameter = 0.300 mm.

Distribution of ThO_2 Particle Sizes

Particle Diameter Range (μm)	Average Particle Diameter (mm)	Weight Percent
0- 44	0.022	17.6
44- 74	0.059	32.2
74-105	0.0895	14.4
105-149	0.127	17.2
149-210	0.1795	14.2
>210	0.250	4.4

TEMPERATURE-DEPENDENT k_∞ CORRELATIONS
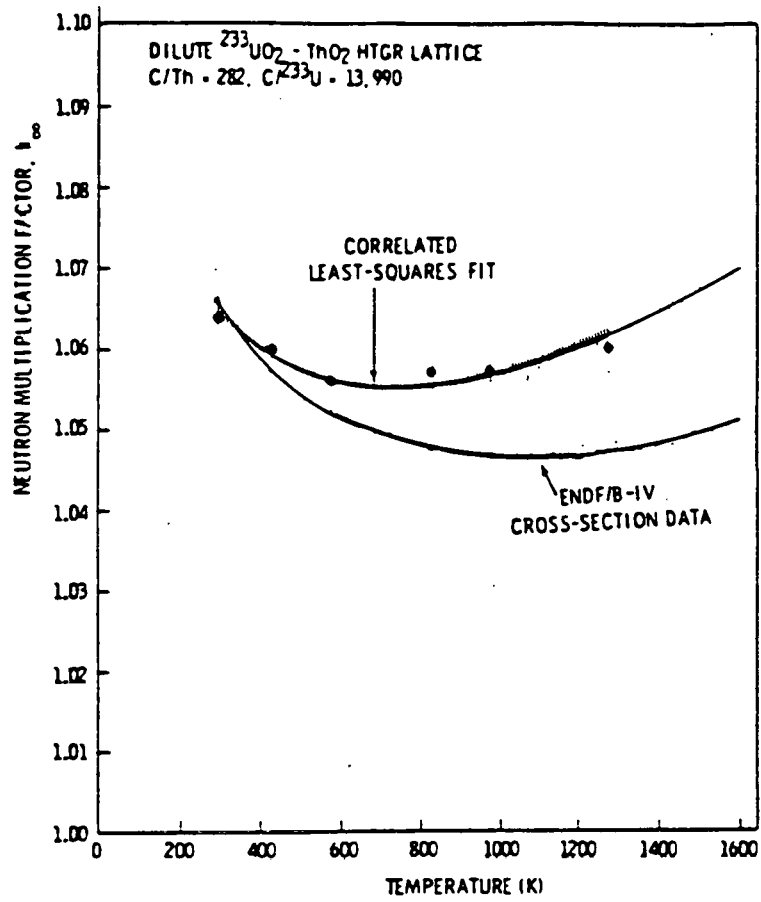
FIGURE 11. Comparison of Calculated and Measured $k_\infty(T)$ Values for HTLTR Lattice 3
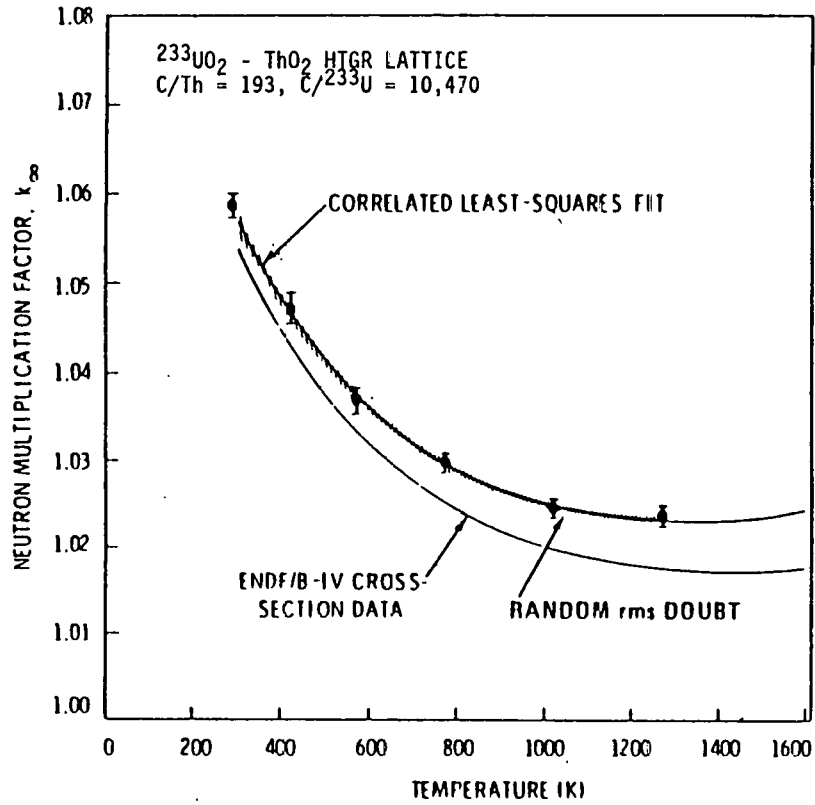
FIGURE 12. Comparison of Calculated and Measured
Neutron Multiplication Factors as a
Function of Temperature for HTLTR
Lattice 2
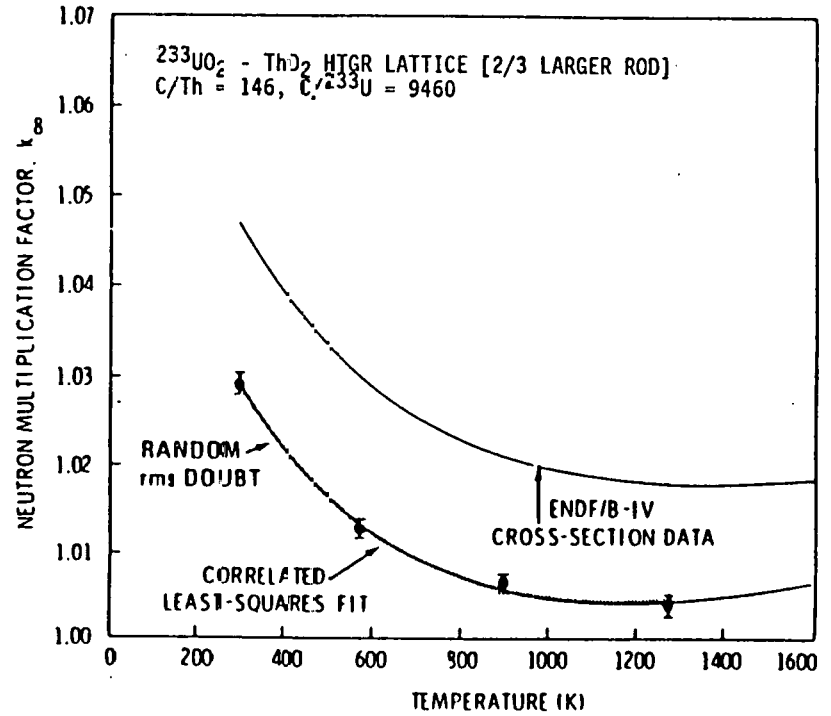
FIGURE 13. Comparison of Calculated and Measured
$k_\infty(T)$ Values for HTLTR Lattice 5

TABLE 6. Experimental and Calculated $k_\infty(T)$ Values for a Dilute $^{233}UO_2$-ThO_2 HTGR Lattice

[C/Th = 282, C/^{233}U = 13,990 (HTLTR Lattice 3); GRANIT/EGGNIT calculations[8] used ENDF/B-IV cross-section data]

Temperature (K)	Experimental Values		Calculated Values
	Measured k_∞	Best Theory Least-Squares-Fit to Measured Data k_∞	All Data from ENDF/B-IV k_∞
293	1.064±0.004	1.0656±0.0011	1.0657
423	1.060±0.006	1.0592±0.0008	1.0573
573	1.056±0.005	1.0560±0.0006	1.0520
823	1.057±0.005	1.0553±0.0007	1.0475
973	1.057±0.006	1.0566±0.0009	1.0465
1273	1.060±0.007	1.0615±0.0012	1.0471
1600	---	---	1.0509

TABLE 7. Experimental and Calculated $k_\infty(T)$ Values for a $^{233}UO_2$-ThO_2 HTGR Lattice

[C/Th = 193, C/^{233}U = 10,470 (HTLTR Lattice 2); GRANIT/EGGNIT calculations[8] used ENDF/B-IV cross-section data]

Temperature (K)	Experimental Values		Calculated Values
	Measured k_∞	Best Theory Least-Squares-Fit to Measured Data k_∞	All Data from ENDF/B-IV k_∞
293	1.0587±0.0014	1.0580±0.0004	1.0544
423	1.0471±0.0017	1.0473±0.0004	1.0428
573	1.0367±0.0014	1.0376±0.0003	1.0334
773	1.0297±0.0011	1.0295±0.0002	1.0251
1023	1.0245±0.0011	1.0248±0.0003	1.0199
1273	1.0237±0.0012	1.0233±0.0004	1.0176
1600	---	---	1.0177

TABLE 8. Experimental and Calculated $k_\infty(T)$ Values for a $^{233}UO_2$-ThO_2 HTGR Lattice (2/3 larger fuel rod)

[C/Th = 146, C/^{233}U = 9460 (HTLTR Lattice 5); GRANIT/EGGNIT calculations[8] used ENDF/B-IV cross-section data]

	Experimental Values		Calculated Values
Temperature (K)	Measured k_∞	Best Theory Least-Squares-Fit to Measured Data k_∞	All Data from ENDF/B-IV k_∞
293	1.0291±0.0012	1.0291±0.0005	1.0473
573	1.0127±0.0010	1.0130±0.0004	1.0301
900	1.0065±0.0010	1.0058±0.0003	1.0211
1273	1.0037±0.0012	1.0043±0.0006	1.0179
1600	---	---	1.0186

Compositions for the PuO_2-ThO_2 HTGR lattice[12] are listed in Table 9; the C/Th atom ratio is about 250 and the C/Pu atom ratio is about 7500. Similar fuel containing PuO_2 microspheres and graphite in the fuel rod region, but with V_2O_3 in place of ThO_2 particles, was used to measure the temperature-dependent k_∞ of this HTGR lattice with the thorium resonance capture removed.[13] The 1/v absorption cross section of vanadium in 273 grams of V_2O_3 just compensates for the 1/v portion of the absorption cross section of thorium in 657 grams of ThO_2 that it replaces in each fuel block. Results of comparisons of experimental and calculated k_∞ values for the PuO_2-ThO_2 HTGR lattice and the PuO_2-V_2O_3 HTGR lattice are shown in Figure 14. Numerical comparisons for the PuO_2-ThO_2 HTGR lattice are listed in Table 10.

Similar measurements were made in the HTLTR with a $^{235}UC_2$-V_2O_3 HTGR lattice.[14] The 1/v absorption cross section of vanadium in 362 grams of V_2O_3 just compensates for the 1/v portion of thorium in 871 grams of ThO_2 that it replaces in a $^{235}UC_2$-ThO_2 HTGR lattice block. Comparison of the $k_\infty(T)$ behavior for the $^{235}UC_2$-V_2O_3 and $^{235}UC_2$-ThO_2 HTGR lattices is shown in Figure 15. At temperatures up to 580 K, the temperature coefficient of reactivity for the $^{235}UC_2$ HTGR lattice (without thorium) is essentially zero.

TABLE 9. Composition of PuO_2-ThO_2 HTGR Lattice

Nuclide	PuO_2 Particles	ThO_2 Particles	Fuel Rod Region	Moderator Region	Homogenized Cell Average
^{238}Pu	1.65-05	--	2.00-08	--	6.17-09
^{239}Pu	1.84-02	--	2.23-05	--	6.88-06
^{240}Pu	5.79-03	--	7.00-06	--	2.16-06
^{241}Pu	8.35-04	--	1.01-06	--	3.12-07
^{242}Pu	2.32-04	--	2.80-07	--	8.64-08
^{244}Pu	2.48-07	--	3.00-10	--	9.25-11
^{241}Am	4.96-05	--	6.00-08	--	1.85-08
^{232}Th	--	2.28-02	9.17-04	--	2.83-04
Oxygen	5.04-02	4.56-02	1.90-03	--	5.86-04
Nitrogen[a]	--	--	2.73-05	1.43-05	1.83-05
Carbon	--	--	4.78-02	8.14-02	7.10-02

(a) At 296 K. For other temperatures, $N_n(T) = N_n(296) \frac{296}{T(K)}$.

C/Th = 251.6, C/Pu = 7541. (HTLTR Lattice 4)
Fuel rod radius = 5.969 mm.
Square lattice pitch = 19.05 mm.
PuO_2 particle diameter = 0.209 mm.

Tyler Standard Screen Mesh	Particle Size Range (μm)	Average Particle Size (μm)	wt%
100- 65	149-210	180	11.1
150-100	105-149	127	16.3
200-150	74-105	90	13.7
325-200	44- 74	59	18.8
>325	0- 44	22	40.1

Thoria Particle Size Distribution
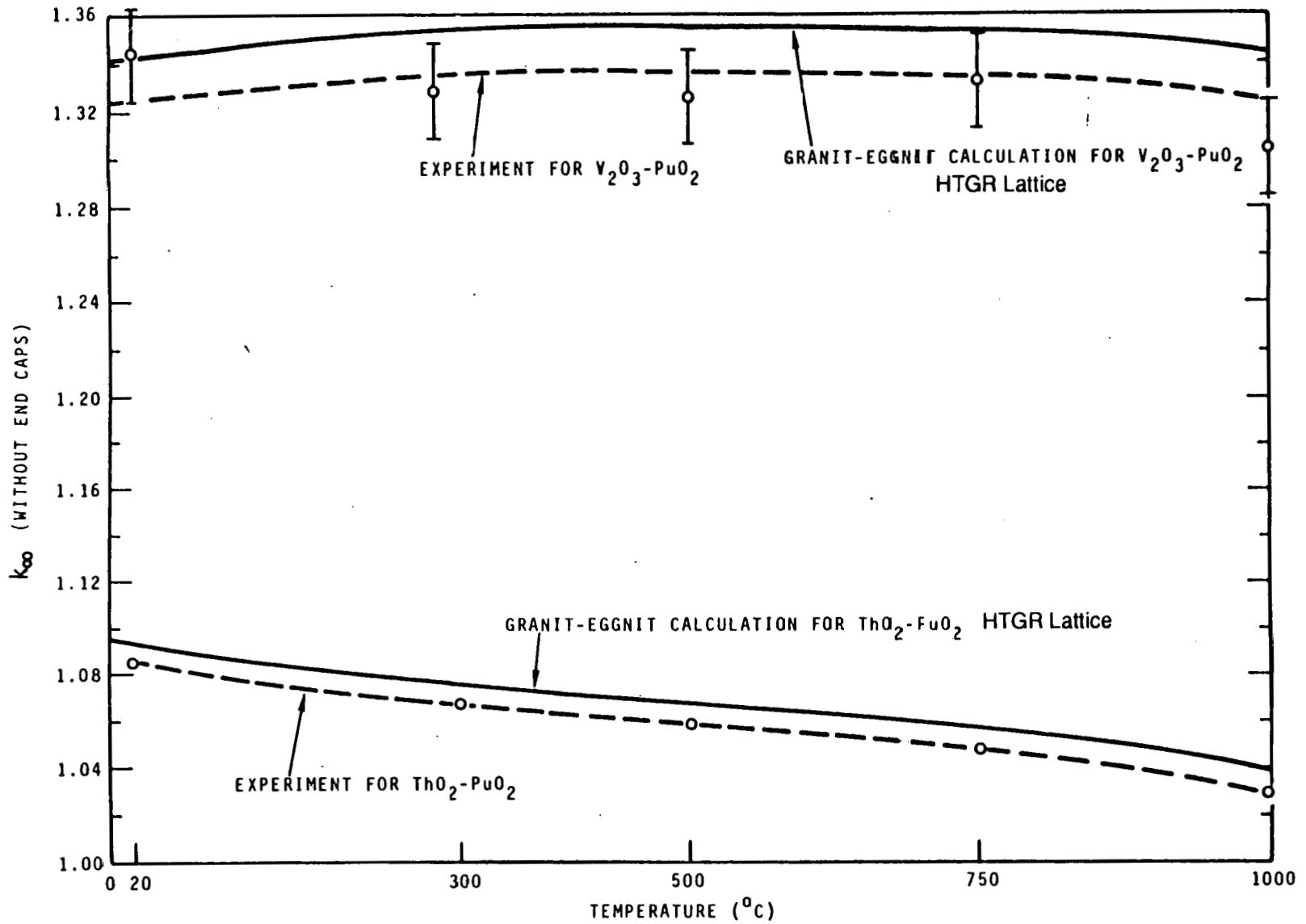
FIGURE 14. Comparison of Calculated and Measured Values of k_∞ for V_2O_3-PuO_2 and ThO_2-PuO_2 HTGR Lattices

TABLE 10. Experimental and Calculated $k_\infty(T)$ Values for a PuO_2-ThO_2 HTGR Lattice

[C/Th = 251.6, C/Pu = 7541 (HTLTR Lattice 4); GRANIT/EGGNIT calculations[13] used ENDF/B-III cross section data]

PuO_2-ThO_2 HTGR Lattice Temperature (K)	Experimental Values		Calculated Values
	Measured k_∞	Best Theory Least-Squares-Fit to Measured Data (k_∞)	All Data from ENDF/B-III (k_∞)
293	1.085±0.003	1.085±0.001	1.092
573	1.067±0.003	1.068±0.001	1.076
773	1.059±0.003	1.060±0.001	1.068
1023	1.048±0.002	1.047±0.001	1.056
1273	1.029±0.002	1.029±0.001	1.039

Analyses of HTLTR reactivity measurements for the $^{235}UC_2$-V_2O_3 HTGR lattice between 580 K and 1273 K were not completed, but the measured data continues the trend established below 580 K.
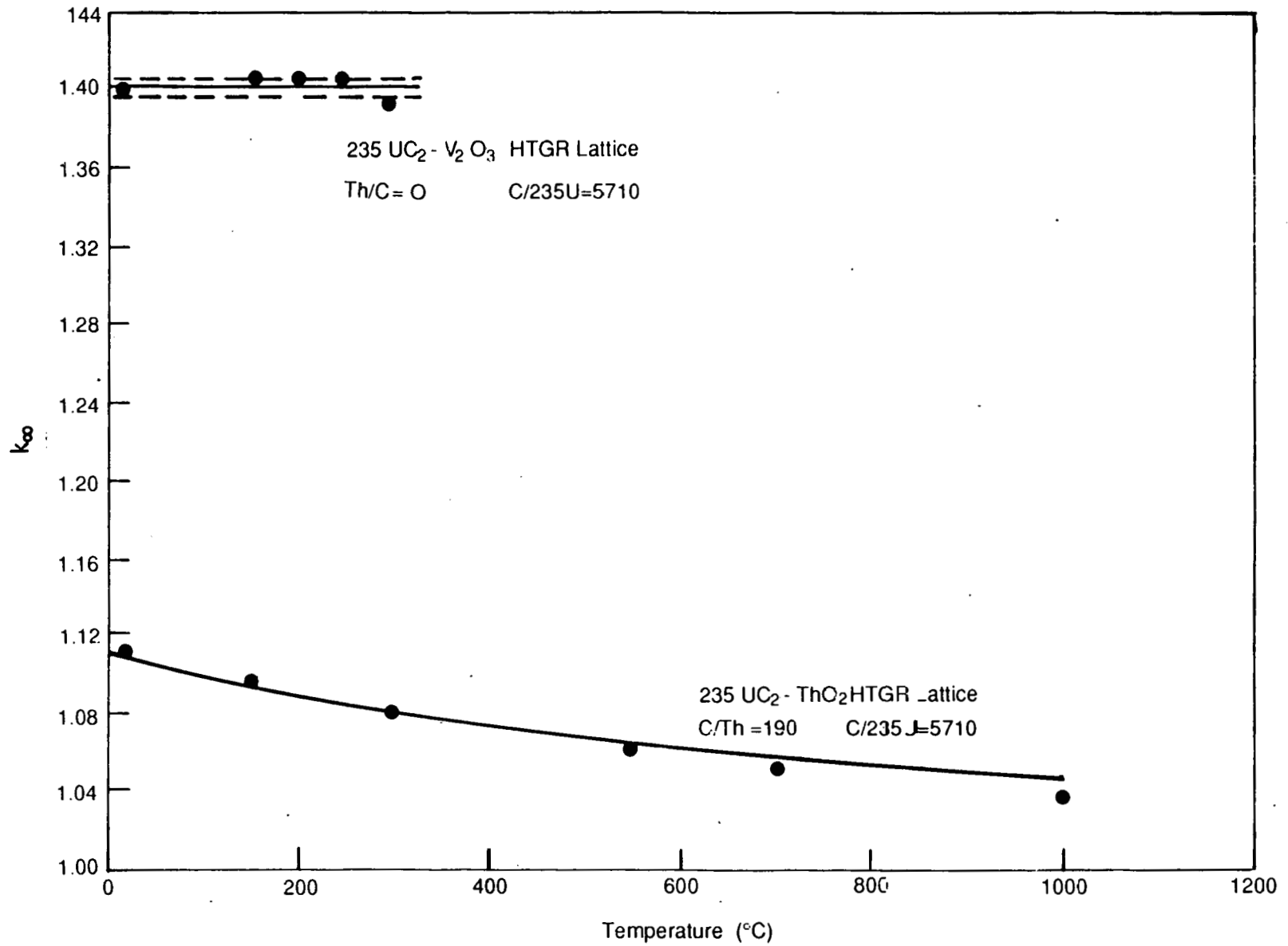
FIGURE 15. Comparison of $k_\infty(T)$ for $^{235}UC_2$-V_2O_3 and $^{235}UC_2$-ThO_2 HTGR Lattices

28

CORRECTIONS OF CALCULATIONAL BIAS

The neutron multiplication factors calculated as a function of temperature, $k_\infty(T)$, for all HTGR lattices tested in the HTLTR, and described in the previous section, have been normalized and rotated to fit the measured values[15] for each experiment by use of the equation

$$\text{Measured}_{k_\infty(T)} = \text{Calculated}_{k_\infty(T)}[A + B(T - 293\text{ K})] \tag{3}$$

The correlation coefficients A and B were determined by a least-squares-fitting procedure using the LEARN computer code.[16] The fitting procedure was performed for results calculated for each different HTGR lattice $k_\infty(T)$ data to determine the effects of the fuel block composition on calculational bias.

Measured and calculated temperature coefficients are related by the equation

$$\text{Meas}\left(\frac{1}{k_\infty}\frac{dk_\infty}{dT}\right) = \text{Calc}\left(\frac{1}{k_\infty}\frac{dk_\infty}{dT}\right) + \frac{B}{A + B(T - 293\text{ K})} \tag{4}$$

In all cases, the value of the correction term is essentially the value of the coefficient B. This is because the order of A is unity, the order of B is 10^{-5}, and T ranges from 293 to 1273 K (20 to 1000°C). Thus, the value of B provides an estimate of the bias correction for calculated temperature coefficients.

The correlation procedure using Eq. (3) was chosen because it minimizes the number of free-fitting parameters, it retains the physical significance of the temperature-dependent shape of the calculations, and because the result fit the measured data well within the estimate of measurement error. Minimization of the number of free parameters is important for reducing the chance of introducing artifacts into the correlation, since there are only six measured values of the k_∞ in the range from 293 to 1273 K (20 to 1000°C) for three of the HTGR experimental lattices. The PuO_2-ThO_2 HTGR experimental

lattice had five measured values of the $k_\infty(T)$ and the $^{233}UO_2$-ThO_2 HTGR lattice with a larger fuel rod had only four measured values of $k_\infty(T)$.

The LEARN program, which was used to fit the coefficients A and B of Eq. (3), calculates the value of chi-squared per degree of freedom from the least-squares fit. This value should be unity if the original random error estimates in the measured data are correct. Since the value of χ^2/η was only ~0.3 for each of the experiments, we can conclude that the original random error estimates were pessimistic.

The correlated least-squares-fit curves to the measured data for $k_\infty(T)$, and the random root-mean-square doubt intervals from the LEARN statistical analysis are shown in Figures 10 through 14 for the five HTGR-fueled HTLTR lattices. Equal weighing of the measured data was used in the least-squares-fitting procedure for HTLTR lattice 3 since the quoted uncertainties in the measured data are dominated by nonuniform systematic error estimates rather than random error estimates (which the least-squares analysis indicates are much smaller than the quoted uncertainty estimates).

The correlation coefficient A of Eq. (3) corresponds to the ratio of the measured-to-calculated values for k_∞ at room temperature and is thus a normalizing coefficient. The coefficient B expresses the bias in the calculated temperature coefficient of reactivity. The values obtained for the correlation coefficients A and B from calculations for each of the HTGR lattices tested in the HTLTR are compared in Table 11. The values of coefficient B obtained from all three $^{233}UO_2$-ThO_2 lattices, indicate that the calculated values of $(1/k_\infty)(dk_\infty/dT)$ are more negative than the measurements. Although these calculations are nonconservative, the magnitude of the bias is relatively small.[15]

The values of the coefficient B obtained for the PuO_2-ThO_2 and the $^{235}UC_2$-ThO_2 are slightly negative, indicating that the calculated temperature coefficient of reactivity is conservative. However, when the thorium is removed, as in the PuO_2-V_2O_3 HTGR lattice, the calculation becomes nonconservative. The trends of the correction to calculated temperature coefficients of reactivity as thorium is removed from the HTGR lattices is shown in Figure 16. For all fissile fuels, the value of B becomes positive when

TABLE 11. Comparison of Least-Squares Correlation Coefficients for $k_\infty(T)$ Values Calculated for Each HTGR Lattice Tested in the HTLTR

| Description of HTGR Lattice Tested in the HTLTR to 1273 K	Least-Squares-Fitted Correlation Coefficients	
	A	B (K^{-1})
$^{235}UC_2$-ThO_2; C/Th = 190; C/^{235}U = 5,710	1.003 ±0.002	-1.07±0.4 x 10^{-5}/K
$^{233}UO_2$-ThO_2; C/Th = 282; C/^{233}U = 13,990	1.000 ±0.001	+1.41±0.19 x 10^{-5}/K
$^{233}UO_2$-ThO_2; C/Th = 193; C/^{233}U = 10,470	1.0034±0.0004	+0.21±0.07 x 10^{-5}/K
$^{233}UO_2$-ThO_2; C/Th = 146; C/^{233}U = 9,460	0.9825±0.0005	+0.41±0.09 x 10^{-5}/K
PuO_2-ThO_2; C/Th = 252; C/Pu = 7,541	0.9932±0.001	-0.24±0.05 x 10^{-5}/K
PuO_2-V_2O_3; Th/C = 0; C/Pu = 7,541	0.978 ±0.003	+0.74±0.6 x 10^{-5}/K
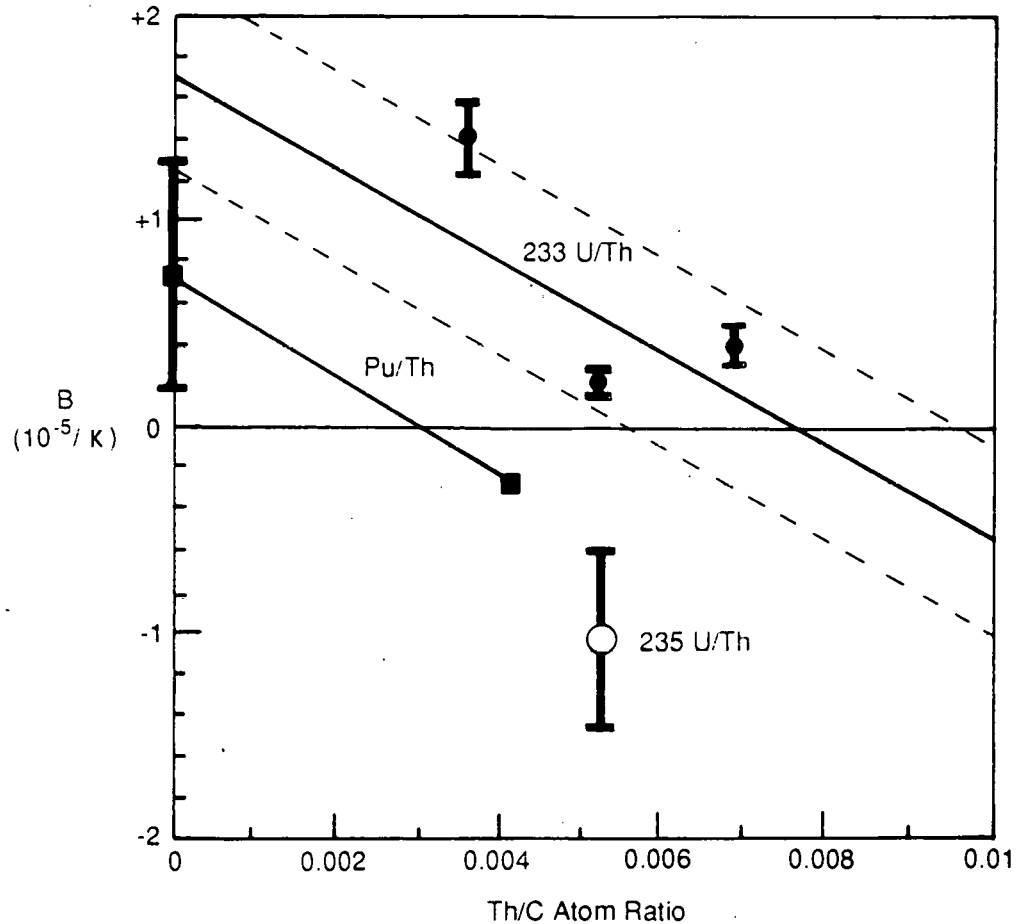
FIGURE 16. Correction of Temperature Coefficient of Reactivity Calculated for HTGR Lattices Using ENDF/B-IV Cross Section Data

31

thorium is absent from the fuel. As a result, the calculated temperature coefficients for HTGR lattices without significant fertile material (Th or ^{238}U) are expected to be nonconservative by 1 to 2 x 10^{-5}/K.

CONCLUSIONS

The values of $k_\infty(T)$ measured in the HTLTR for five HTGR test cores provide a consistent set of benchmark data that can be used to validate unit cell calculations of doubly heterogeneous HTGR lattices. The neutron spectrum averaged self-shielding effects of both the fissile and fertile fuel particles, as well as thermal neutron spectrum variations in the fuel rod surrounded by graphite moderator, and the rod-to-rod resonance shielding effects must be accurately accounted for in calculations to be compared with the HTGR lattice measurements. Unit cell calculations must be made using the fundamental mode neutron spectrum generated in a just critical bare array of the test material, to be consistent with the measurement conditions. Such PNL calculations made with GRANIT/EGGNIT using ENDF/B-IV cross-section data for comparison to the measured $k_\infty(T)$ values show that:

- Absolute values of k_∞ can be calculated within about 1% of the measured values at room temperature.

- The differences between calculated and measured values of k_∞ are larger than can be accounted for by the 1% uncertainty in the fissile content of the coated microspheres.

- Calculated values of k_∞ for the most heterogeneous lattice (HTLTR Lattice 5) are nearly 2% higher than measured values, indicating overestimation of resonance shielding and/or underestimation of thermal flux depression in the fuel region. This lattice is more sensitive to the latter effect.

- The HTLTR data provides accurate benchmarks for determining the magnitude of bias in calculated temperature coefficients of reactivity for HTGR lattices.

- Calculations of temperature coefficients of reactivity for all three ^{233}U fueled HTGR lattices were non-conservative (more negative than measured).

- The trend, as thorium was removed from HTGR lattices, was to calculate temperature coefficients that were more non-conservative.

- The non-conservative bias in calculated temperature coefficients of reactivity for HTGR lattices tested in the HTLTR was 1 to $2 \times 10^{-5}/K$ when thorium was not present.

In order to increase measurement accuracy by keeping k_∞ less than 1.1, the HTLTR experiments used HTGR fuel loadings that contained only about one-half to one-third of the fissile fuel concentration in typical fresh commercial HTGR cores such as that shown in Figure 2. Increased fissile fuel concentrations may amplify calculational errors in underestimation of thermal flux depression in the fuel region and lead to larger errors in calculation of $k_\infty(T)$ than indicated by comparisons to HTLTR measurements. Measurements on a $^{235}UC_2$-fueled HTGR lattice (without thorium) in the HTLTR (shown in Figure 15) indicate that the temperature coefficient of reactivity for such compositions is essentially zero. A 1/v neutron absorber (V_2O_3) was present in the fuel in a concentration that provided a 1/v neutron cross section equivalent to the thorium it displaced. The effect of lumped 1/v neutron absorbers outside the HTGR unit cell, such as boron control rods used in FSV, on the temperature coefficient of reactivity may be negative since thermal neutron self-shielding effects are reduced as temperature increases. However, the reactivity feedback from such isolated absorbers may not provide the prompt reactivity feedback necessary for HTGR power stability and transient response due to the time lag for heat transfer from the fuel to the absorber.

REFERENCES

1. Dahlberg, R. C., R. F. Turner, and W. V. Goeddel. 1974. "HTGR Fuel and Fuel Cycle Summary Description." GA-A12801, Rev., General Atomic Company, LaJolla, California.

2. Holmes, J. A. G. 1961. "Specification for HERO--A Low Power High Temperature Experimental Reactor." DEG-345(R), U. K. Atomic Energy Authority, Risley.

3. Department Des Etudes De Piles, Commissariat a l'Energie Atomique. 1961. "Empilement Critique Chaud--CESAR." Rapport DEP No. 13.

4. Reynolds, H. L. and C. E. Walter. 1959. "HOT BOX--A High Temperature Critical Facility." UCRL-5483, Lawrence Livermore Laboratory, Livermore, California.

5. Bennett, C. L. 1971. "GRANIT: A Code for Calculating Position Dependent Thermal Neutron Spectra in Doubly Heterogeneous Systems by the Integral Transport Method." BNWL-1634, Pacific Northwest Laboratory, Richland, Washington.

6. Richey, C. R. 1969. "EGGNIT: A Multigroup Cross Section Code." BNWL-1203, Pacific Northwest Laboratory, Richland, Washington.

7. Richey, C. R. and T. J. Oakes. 1972. "Determination of Neutron Multiplication Factors as a Function of Temperature with the High Temperature Lattice Test Reactor." Nucl. Sci. Eng., 47:40.

8. Newman, D. F., et al. 1977. "Evaluation of Temperature Coefficients of Reactivity for ^{233}U--Thorium Fueled HTGR Lattices." EPRI NP-222, Electric Power Research Institute, Palo Alto, California.

9. Oakes, T. J. 1972. "Measurement of k_∞ as a Function of Temperature for a $^{233}UO_2$-$^{232}ThO_2$-C Lattice." BNWL-1601, Pacific Northwest Laboratory, Richland, Washington.

10. Lippincott, E. P. 1972. "Measurement of the Temperature Dependence of k_∞ for a $^{233}UO_2$-ThO_2 High Temperature Gas-Cooled Reactor Lattice." Nucl. Sci. Eng., 47:475.

11. Lippincott, E. P. 1972. "Measurement of Physics Parameters for a MSBR Lattice in the HTLTR." BNWL-1633, Pacific Northwest Laboratory, Richland, Washington.

12. Newman, Darrell F. 1973. "Temperature-Dependent k_∞ for a ThO_2-PuO_2 HTGR Lattice." Nucl. Technol., 19:66.

13. Newman, Darrell F. 1972. "Measurement of Neutronic Parameters for a Plutonium Fueled HTGR Lattice." BNWL-1678, Pacific Northwest Laboratory, Richland, Washington.

14. Lanning, D. D. 1969. "High Temperature Reactor Physics Program - Status Report." BNWL-CC-2096. Pacific Northwest Laboratory, Richland, Washington.

15. Newman, D. F. and B. F. Gore. 1978. "Neutron Multiplication Factors as a Function of Temperature: A Comparison of Calculated and Measured Values for Lattices Using $^{233}UO_2$-ThO_2 Fuel in Graphite." Nucl. Technol. 37:227.

16. Seybold, G. D. 1969. "Users Aid: Programs LEARN and LIKELY." BNWL-1057, Pacific Northwest Laboratory, Richland, Washington.

17. Heineman, R. E. 1965. "On the Interpretation of Reactivity Measurements of Reactor Media." Trans. Am. Nucl. Soc. 8:532.

18. Lippincott, E. P. et al. 1969. "Definition of the Infinite Neutron Multiplication Factors Measured by the PCTR Poisoned and Unpoisoned Technique," Reactor Physics Quarterly Report, July, August, September, BNWL-1240, Pacific Northwest Laboratory, Richland, Washington.

19. Lippincott, E. P. 1971. "Derivation of Corrections of k_∞ in the Two-Group Approximation," BNWL-1560, Pacific Northwest Laboratory, Richland, Washington.

20. Newman, D. F. 1971. "An Improved Method for Calculating Foil Perturbation Effects," Nucl. Sci. Eng., 44:261.

21. Lippincoff, E. P. 1971. "Measurement of the Temperature Dependence of k_∞ for a $^{233}UO_2$-ThO_2 HTGR Lattice." BNWL-1561, Pacific Northwest Laboratory, Richland, Washington.

22. Hanthorn, H. E. 1966. "Final Safeguards Analysis: High Temperature Lattice Test Reactor." BNWL-CC-225, Pacific Northwest Laboratory, Richland, Washington.

23. Little, W. W. and Hardie, R. W. 1969. "2DB Users Manaul - Revision 1." BNWL-831, Pacific Northwest Laboratory, Richland, Washington.

APPENDIX A

PRINCIPLE OF THE MEASUREMENTS

DO NOT MICROFILM
THIS PAGE

APPENDIX A

PRINCIPLE OF THE MEASUREMENTS

The primary neutronic characteristic of a test lattice that is measured in the High Temperature Lattice Test Reactor (HTLTR), shown in Figure 1, is the infinite medium neutron multiplication factor, k_∞, as a function of temperature.[7]

The measured quantity is not for a true infinite medium, but rather for a bare critical reactor. Thus, k_∞ is evaluated for neutron flux spectra in the fundamental mode. To avoid ambiguity, k_∞ is defined by

$$k_\infty = \frac{\text{total production}}{\text{total absorption}} \cdot \tag{A.1}$$

This quantity can be calculated directly for comparison to measured quantities using multigroup cell codes.

$$k_\infty = \sum_{i=1}^{n} \left(\nu_i \Sigma_{f_i} \phi_i \right) / \sum_{i=1}^{n} \left(\Sigma_{a_i} \phi_i \right) \tag{A.2}$$

where ϕ_i = i'th group neutron flux at the center of a just critical bare assembly of the test lattice, and $\nu_i \Sigma_{f_i}$ and Σ_{a_i} are cell-averaged macroscopic neutron production and absorption cross sections, respectively, in the i'th energy group.

For simplicity these fundamental mode spectrum averaged cross sections can be collapsed into two energy regions, and the expression becomes.[a]

(a) k_∞ as defined in this paper is equivalent to $k_\infty^\dagger$ as defined in reference 7 and k_∞' as defined in reference 18. The fluxes, ϕ_1, ϕ_2, in this paper are equivalent to ϕ_1', ϕ_2' as defined in references 7 and 18. The primes have been deleted herein for simplicity of notation.

$$k_\infty = \frac{\nu_1 \Sigma_1^f \phi_1 + \nu_2 \Sigma_2^f \phi_2}{\Sigma_1^a \phi_1 + \Sigma_2^a \phi_2} ,$$

(A.3)

where subscript 2 represents the thermal region and subscript 1 represents the epithermal region. These quantities are also related by the two-group equations

$$-D_1 B^2 \phi_1 - \Sigma_1^a \phi_1 - \Sigma_{12} \phi_1 + \nu \Sigma_1^f \phi_1 + \nu \Sigma_2^f \phi_2 = 0$$

(A.4a)

$$-D_2 B^2 \phi_2 - \Sigma_2^a \phi_2 + \Sigma_{12} \phi_1 = 0 ,$$

(A.4b)

where Σ_{12} is the cross section for transfer from group 1 to group 2 and B^2 is the material buckling.

The fundamental mode neutron fluxes in Eq. (A.4) can be eliminated by defining the following lattice parameters:

$$\tau = \frac{D_1}{\Sigma_1^a + \Sigma_{1 \to 2}}$$

(A.5)

$$L^2 = \frac{D_2}{\Sigma_2^a}$$

(A.6)

$$\eta_1 f_1 = \frac{\nu \Sigma_1^f}{\Sigma_1^a} , \quad \eta_2 f_2 = \frac{\nu \Sigma_2^f}{\Sigma_2^a}$$

(A.7)

$$p = \frac{\Sigma_{1 \to 2}}{\Sigma_{1 \to 2} + \Sigma_1^a}$$

(A.8)

Substituting these terms into Eqs. (A.3) and (A.4) gives

A.2

$$k_\infty = \frac{\eta_1 f_1 (1 - p)(1 + L^2 B^2) + \eta_2 f_2 p}{1 + (1 - p)L^2 B^2}$$

(A.9)

where, B^2 is the material buckling of the test lattice which is equivalent to the fundamental mode (geometric) buckling for a just critical array of the test lattice.

$$k_{eff} = 1 = \frac{k_\infty [1 + (1 - p) L^2 B^2]}{(1 + \tau B^2)(1 + L^2 B^2)}$$

(A.10)

A rearrangement of Eq. (A.10) illustrates the relationship between k_∞ and the fundamental mode buckling, B^2.

$$k_\infty = \frac{(1 + \tau B^2)(1 + L^2 B^2)}{1 + (1 - p)L^2 B^2} \quad .$$

(A.11)

The excess neutron production in the test lattice, $k_\infty - 1$, is determined from the ratio of reactivity perturbations of a test lattice sample and a normalizing neutron absorber, using the unpoisoned technique.[17] A small sample of the test lattice (referred to as the central cell) is inserted to fill the void in the center of the HTLTR. Surrounding this void is a region of test lattice identical to the central cell, and the neutron spectrum in this region is adjusted to be as close as possible to the fundamental mode condition.[18] The reactivity perturbation caused by insertion of the central cell is normalized to the perturbation produced when a sample of copper is placed in the central void of the HTLTR.

Using first order perturbation theory and the fundamental mode neutron spectrum collapsed to two-energy-groups, the relationship between k_∞ and the measured quantities can be derived:[18,19]

$$k_\infty = 1 - \left[\frac{\Delta\rho^{cell}}{\Delta\rho^{Cu}}\right] \frac{(\Sigma_a \phi V)_2^{Cu}}{(\Sigma_a \phi V)_2^{Cell}} \left[1 + \left(\frac{\phi_1^\dagger}{\phi_2^\dagger}\right) \frac{(\Sigma_a \phi)_1^{Cu}}{(\Sigma_a \phi)_2^{Cu}}\right]$$

$$- \frac{(1 + \tau B^2)(1 + L^2 B^2)(1 - p)L^2 B^2}{1 + (1 - p)L^2 B^2} + \frac{\tau B^2 (1 + L^2 B^2)\left[\tau B^2 - \eta_1 f_1 (1 - p)\right]}{1 + \tau B^2 - \eta_1 f_1 (1 - p)}$$

$$- \frac{(\tau B^2 (1 + L^2 B^2)}{1 + \tau B^2 - \eta_1 f_1 (1 - p)} \left[\frac{\Delta\Phi}{\Phi} + \frac{\Delta\Phi^\dagger}{\Phi^\dagger}\right]$$

$$+ \frac{(1 + L^2 B^2)\left[1 - \eta_1 f_1 (1 - p)\right]}{1 + \tau B^2 - \eta_1 f_1 (1 - p)} \left[\frac{\Delta\Phi}{\Phi} \frac{\Delta\Phi^\dagger}{\Phi^\dagger}\right] \tag{A.12}$$

In Eq. (A.12), $\Delta\rho^{cell}$ and $\Delta\rho^{Cu}$ represent the reactivity changes due to insertion of the central cell or copper into the void, respectively; $(\Sigma_2^a V \phi_2)^{cell}$ represents the actual thermal-neutron absorption rate in the central cell; $(\Sigma_2^a V \phi_2)^{Cu}$ represents the actual thermal-neutron absorption rate in the copper; and $(\Sigma_a \phi)_1^{Cu}/(\Sigma_a \phi)_2^{Cu}$ represents the ratio of epithermal-to-thermal absorption rates in the copper placed in the central HTLTR void. Neutron absorption rates in the central cell constituents and the copper were measured by foil activation methods, and corrected for foil perturbation effects.[20]

The first term in this expression is the preponderant term for thermal spectrum test lattices, and is evaluated experimentally. The next two terms are small calculated corrections which account for fundamental mode neutron leakage effects from the central cell. The last two terms in Eq. (A.12) are calculated two-group corrections for neutron spectrum mismatch from funda-mental mode values, where Φ is defined as ϕ_1/ϕ_2 and $\Delta\Phi$ is the difference between Φ for the fundamental mode and the Φ actually present with the central cell inserted; $\Phi^\dagger$ is defined similarly for the adjoint fluxes except $\Delta\Phi^\dagger$ is evaluated at the surface of the void.

Since the fundamental mode buckling, B^2, is not measured directly and cannot be calculated to the desired accuracy, B^2 is evaluated using the experimental value of k_∞ from Eq. (A.12) via the relation in Eq. (A.11). It was necessary to iterate on the buckling value from Eq. (A.11) in calculations of lattice parameters defined in Eq. (A.5) through (A.8). These methods eliminate errors in the buckling due to uncertainties in the fuel block loading, heterogeneous geometry, and limitations of calculational methods.

The HTLTR experiments were designed to make use of the tremendous power of Eq. (A.12) to determine k_∞ -1 and therefore k_∞ to a high degree of accuracy. In all five of the HTGR lattice experiments, the calculated terms contribute less than 10% to k_∞ -1. Therefore if the sum of these terms were estimated within 10%, they contributed less than 1% error in k_∞ -1. Reaction rate ratios were measured within a 2% uncertainty, and the uncertainties in the neutron spectrum mismatch for k_∞ near unity limit the minimum error to about 0.001. So, the overall uncertainty in k_∞ -1 was about 4%. For a typical k_∞ of 1.08 the overall uncertainty is only 0.003, or 0.3%. No other method utilizing only a small portion of a critical mass approaches this range of accuracy.

Another advantage of the formulation in Eq. (A.12) is that only thermal absorption rates in the central cell constituents must be evaluated from foil activation measurements to determine k_∞. The uncertainties involved in evaluating epithermal resonance absorption rates in the fuel and epithermal capture-to-fission ratios in fissionable materials were eliminated. In addition it should be noted that except for the errors in measuring reactivity perturbations, $\Delta\rho$, all other uncertainties in k_∞ -1 were systematic with changes in temperature. Therefore the uncertainty in $[k_\infty(T_2) - k_\infty(T_1)]$ was also about 4%, and in fact was less than the overall uncertainty in k_∞.

The formulation in Eq. (A.12) has general limitations which were evaluated to substantiate its applicability to the particular HTGR lattice situations. For HTGR and other thermal spectrum test lattices, the thermal and epithermal neutron leakage correction terms are an order of magnitude smaller than the experimentally evaluated term which is normalized by thermal

neutron absorption rates. If the test lattice is nonthermal, $p \rightarrow o$ and $\eta_1 f_1 \rightarrow k_\infty$, the epithermal leakage correction becomes prohibitively large and a different formulation is required.

The evaluation of k_∞ in the fundamental mode has the advantage of unique fluxes regardless of the multi-group neutron energy structure used. If there is insufficient test lattice surrounding the center cell to establish these unique fluxes within the epithermal and thermal groups, or if a dissimilar test lattice surrounds the center cell, the two-group mismatch corrections given in Eq. (A.12) would be inappropriate. For those cases, a more general multi-group equation must be used to evaluate k_∞, with some sacrifice in accuracy. It is not necessary to mockup the entire HTLTR to calculate $k_\infty(T)$ values for comparison to the experimental values. Only a bare critical assembly of the test material must be mocked up to calculate k_∞ in the fundamental mode at each measurement temperature. However, it was necessary to mockup the entire HTLTR to calculate the small correction terms for neutron flux and adjoint spectral mismatch in the central cell void. The details on the reactor loadings that were necessary to make these entire HTLTR calculations are given in the original PNL reports for each experiment (see references 7, 9, 11, 13, 14, and 21).

APPENDIX B

EXPERIMENTAL PROCEDURES

APPENDIX B

EXPERIMENTAL PROCEDURES

Detailed descriptions of the experimental procedures used in the HTLTR for each of the five HTGR lattice test cores are provided in the original PNL reports for those experiments (see references 7, 9, 11, 13, 14, and 21). A summary description of those procedures is provided here for completeness.
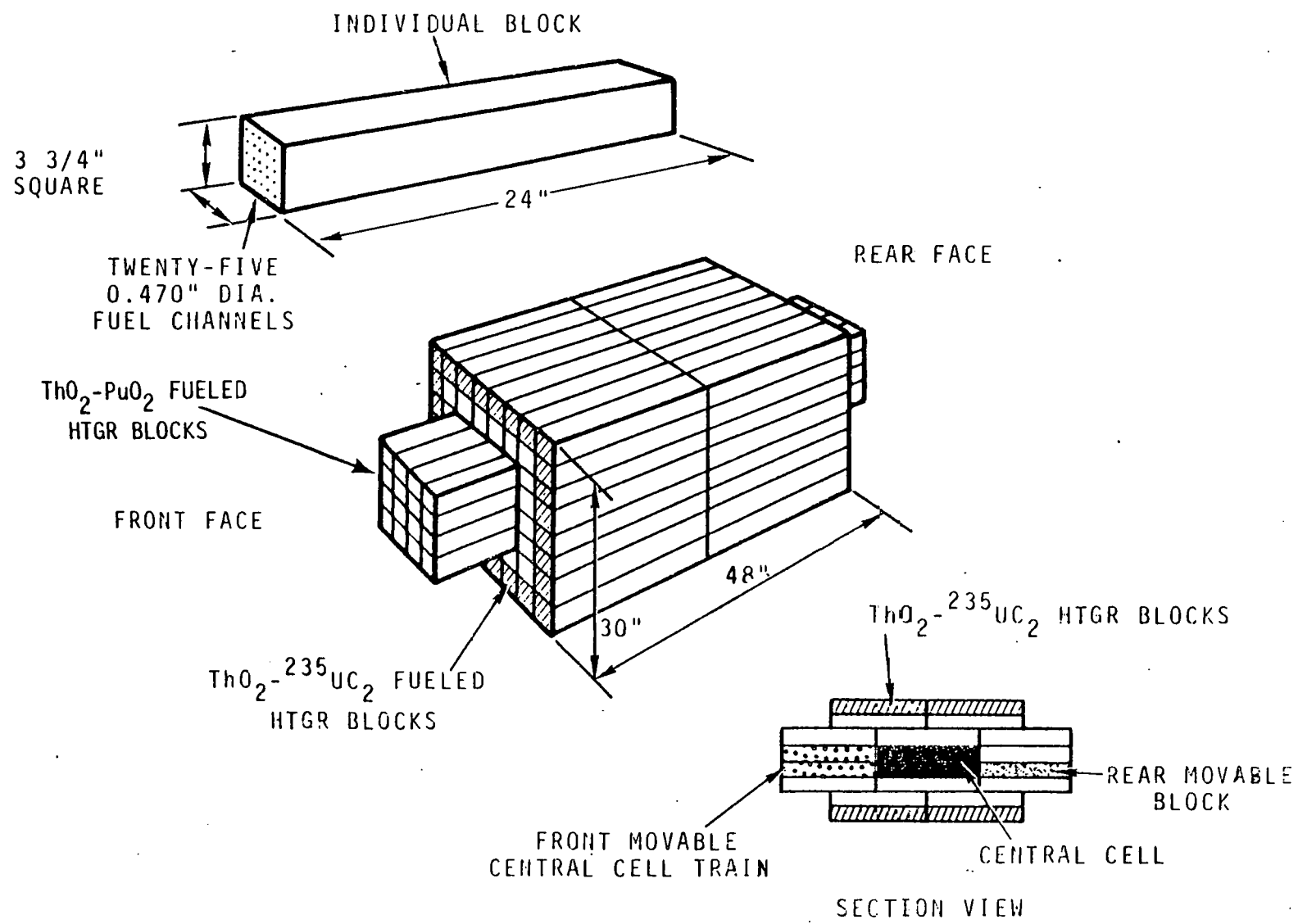
TEST LATTICE CONFIGURATION

Each HTGR test lattice in the HTLTR was arranged similar to that shown in Figure B.1 for the ThO_2-PuO_2 HTGR test lattice. the HTGR fuel blocks were loaded into the center of the HTLTR in an 8 x 8 array. The outer two rows of blocks are 4-ft in length; the inner 4 x 4 array of HTGR blocks are 6-ft in length. External to the test lattice, the HTLTR was loaded with short end drivers adjacent to the ends of the test lattice and, radially, with driver fuel buffer fuel, and temperature compensating shims[22] as appropriate to provide sufficient reactivity for reactor operations and to adjust the neutron spectrum incident on the test lattice.

NEUTRON SPECTRUM MATCHING

The required reactivity measurements in the central void of the HTLTR were made with a reactor loading where the neutron spectrum in the vicinity of the central test cell was nearly the same as in a bare critical array of the test lattice.

To determine the reactor configuration external to the test lattice likely to give a good flux match in the vicinity of the central test cell, calculations were made using the two-dimensional diffusion theory code 2DB[23] and a two-energy-group model of the HTLTR in R - Z geometry. The lattice spectrum was matched when the thermal-to-epithermal flux ratio in the region adjacent to the central cell is the same as in the central cell. Spatial variations of the neutron spectrum were measured throughout the HTLTR using bare and cadmium-covered gold foils. The neutron spectrum index (gold

INDIVIDUAL BLOCK

3 3/4" SQUARE

24"

TWENTY-FIVE 0.470" DIA. FUEL CHANNELS

ThO_2-PuO_2 FUELED HTGR BLOCKS

REAR FACE

FRONT FACE

48"

30"

ThO_2-$^{235}UC_2$ FUELED HTGR BLOCKS

ThO_2-$^{235}UC_2$ HTGR BLOCKS

REAR MOVABLE BLOCK

FRONT MOVABLE CENTRAL CELL TRAIN

CENTRAL CELL

SECTION VIEW

FIGURE B.1. ThO_2-PuO_2 HTGR Test Lattice (Central Region of HTLTR)

cadmium ratio-1) is directly proportional to the thermal-to-epithermal flux ratio. An example of the comparison of measured and calculated (gold cadmium ratio-1) values in the radial direction, shown in Figure B.2, and in the axial direction, shown in Figure B.3, indicate excellent agreement. Similar good agreement was obtained for the other HTGR test lattices. These results provide validation of the 2DB calculations for the entire HTLTR that were used to provide reasonable estimates of two-group flux mismatch corrections for the k_∞ measurements. In addition, to minimize axial streaming, the neutron flux level in the HTLTR was flattened in the axial direction as illustrated in Figure B.4. To change the neutron flux level and spectrum, driver fuel and gadolinium shims were adjusted in the radial and axial regions of the HTLTR surrounding the test lattice.

Measurement of Reaction Rates

The measurement of relative thermal reaction rates in the actual cell and copper absorber was carried out at room temperature using foils. These foils were normalized to foils placed on a rotator at a location near the edge of the HTLTR. The rotator ensures that each type of foil sees an identical flux.

The reaction rate in the copper poison was measured by placing the poison strips in the cavity left when the central cell was removed and irradiating the material. Foils were punched from selected locations in the strips and the copper activity determined, to obtain the integral of absorptions in the poison strips.

The cell reaction rate was measured using 0.005-inch copper foils to evaluate 1/v absorptions and fuel foils to evaluate fuel absorption. The copper foils were placed axially and radially between the central cell blocks to allow an integral of the flux over the cell to be calculated. A special fuel block, shown in Figure B.5, containing the same HTGR fuel mixture as the central cell blocks was used to hold foils for the reaction rate measurements. This block had the fuel in two channels contained in removable aluminum cylinders, three in each channel, between which foils could be inserted. Special foils were fabricated to fit in the fuel channels. Foils made of copper and foils containing a mixture of coated fissile fuel
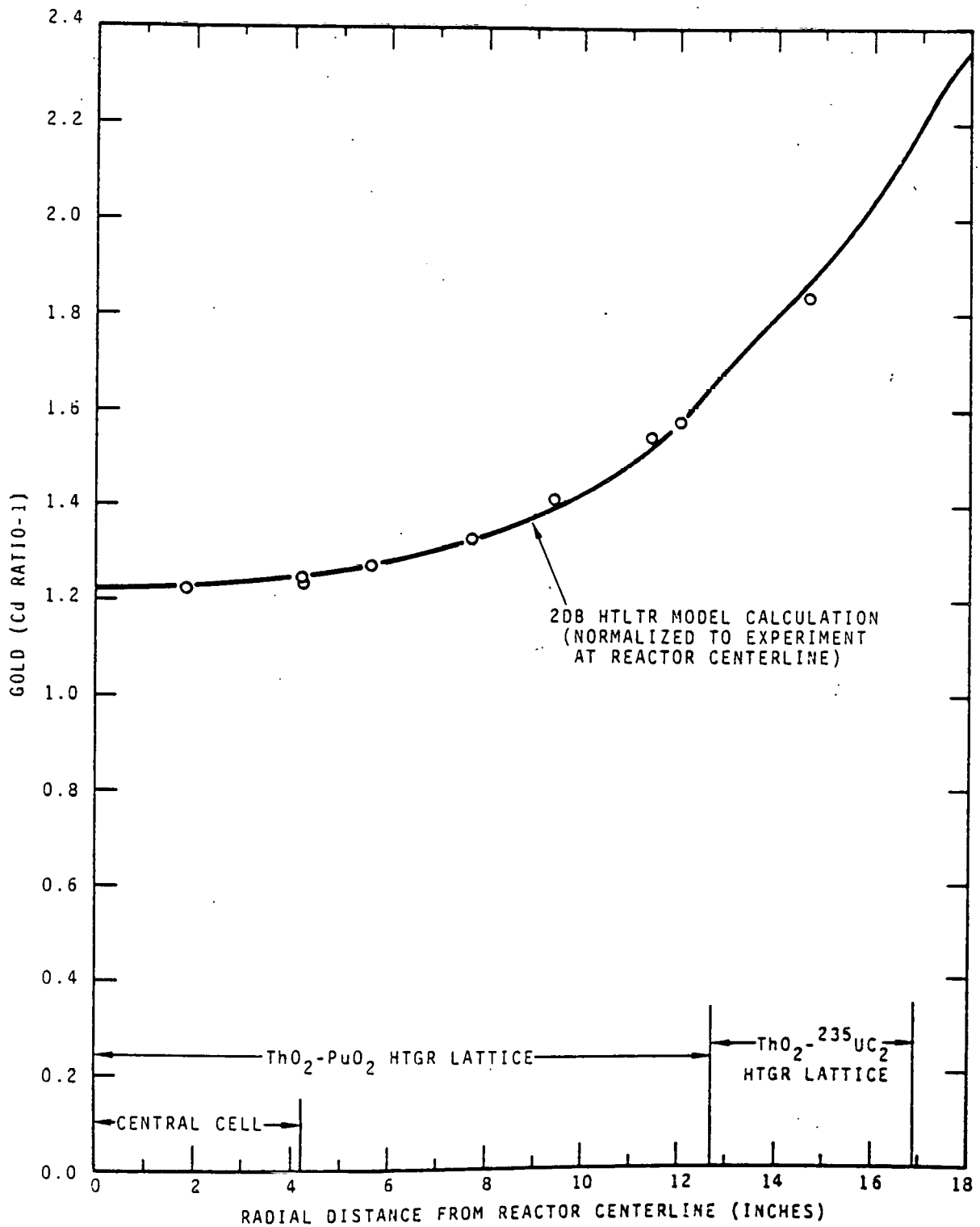
B.3

FIGURE B.2. Comparison of Measured and Calculated (Gold Cadmium Ratio -1) as a Function of Radial Distance from the Reactor Centerline

B.4
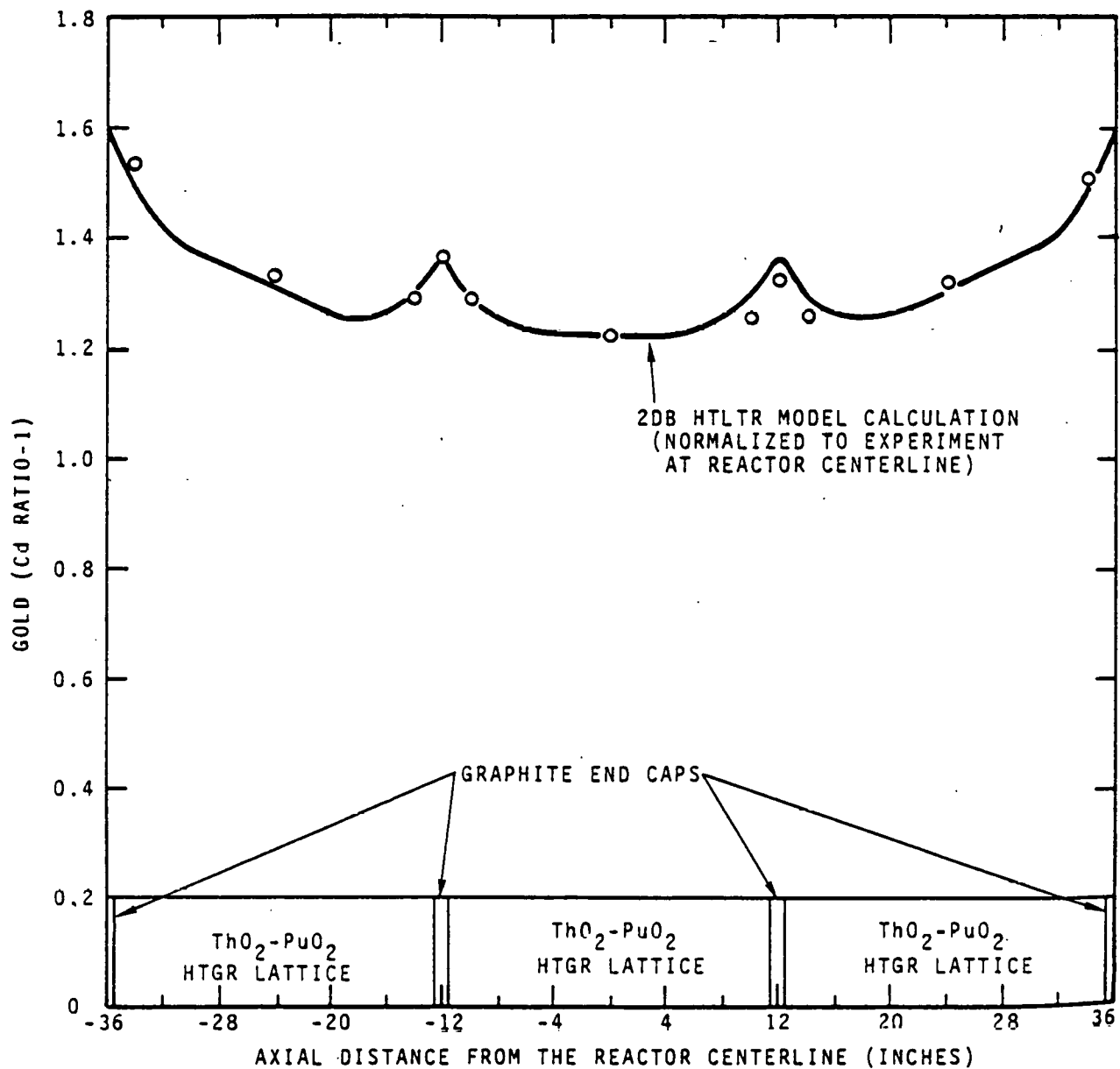
FIGURE B.3. Comparison of Measured and Calculated (Gold Cadmium Ratio -1)
as a Function of Axial Distance from the Reactor Centerline

microspheres, ThO_2 particles, and graphite identical to the test lattice fuel
were used. These fuel foils were used to evaluate the relative absorption
rates in fissile fuel and thorium.

In order to evaluate relative thermal absorptions, both bare and
cadmium-covered (0.040-inch thick cadmium) foils were irradiated. The

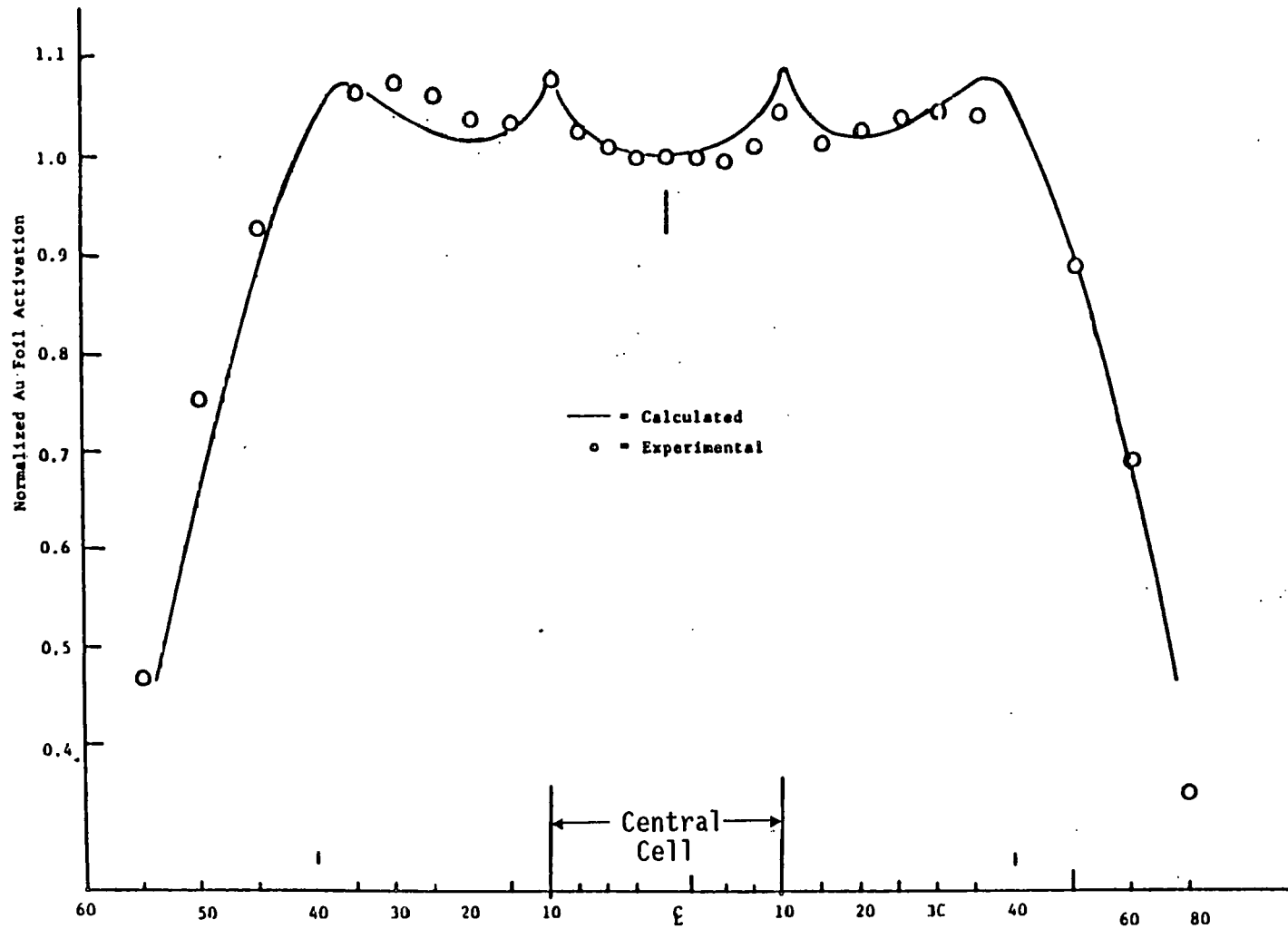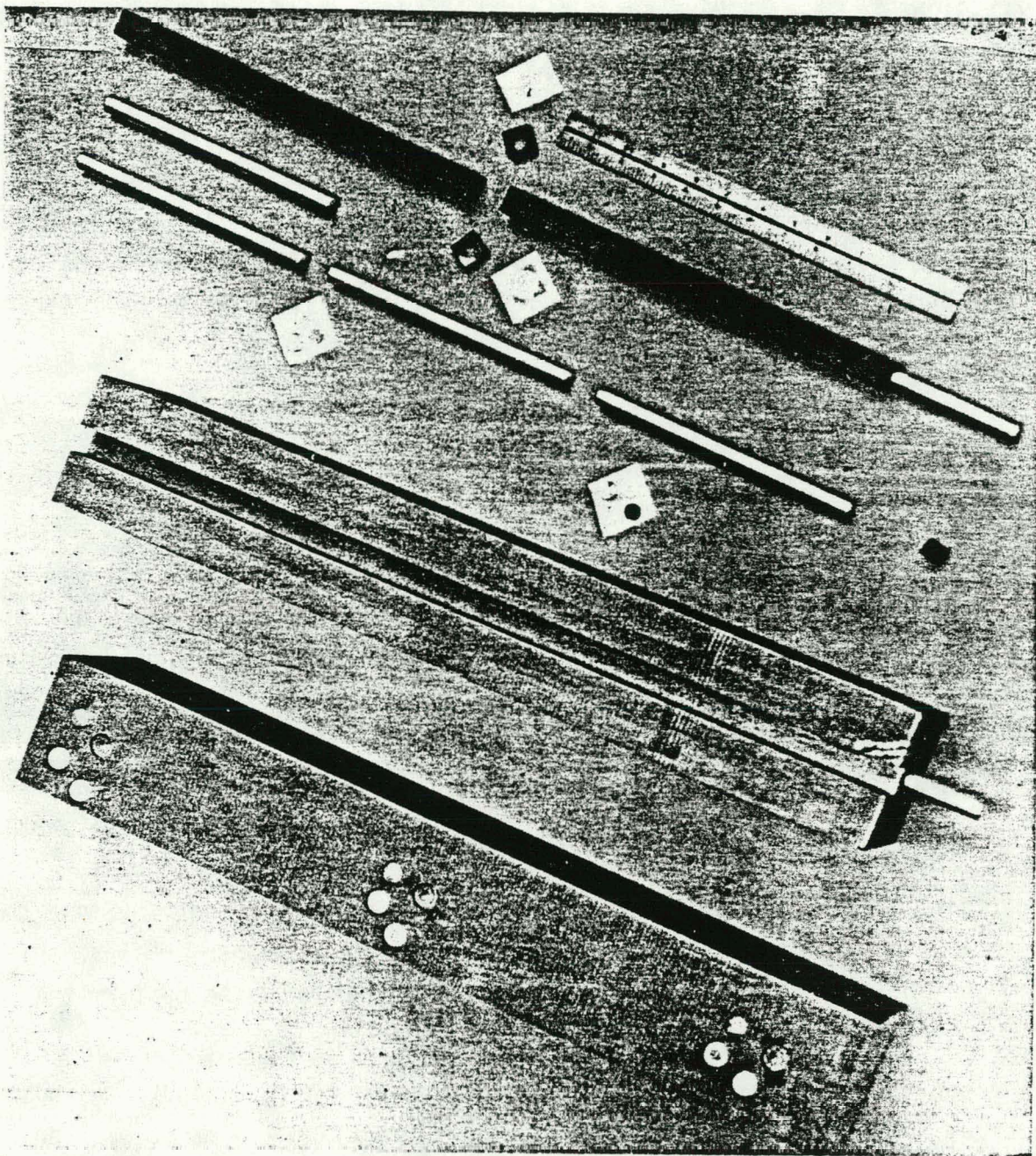FIGURE B.4. Bare Gold Axial Traverse

FIGURE B.5. Special HTGR Fuel Block Used in Foil Irradiations

measured relative reaction rates were then corrected for the perturbations caused by the aluminum, the foils, and cadmium covers.[20] These corrections were calculated using the two-dimensional transport theory code DOTSN.[12] The corrections to the bare activity were small (about 0.5% or less). The

B.7

corrections for the cadmium cover perturbations were larger, however. These perturbations arise from depression of the epithermal flux in the vicinity due to thermal absorption in the cadmium, epithermal absorption in the cadmium, and due to production of thermal neutrons by scattering inside the cadmium cover. The DOTSN calculation provides the thermal and epithermal flux inside the cadmium cover relative to the unperturbed flux far from the foil. For example, the thermal and epithermal activation rates in the PuO_2-ThO_2 HTGR fuel were evaluated, using the DOTSN results by the relations:

$$A_{Thermal} = 1.004 \ A^{bare} - 1.036 \ A^{Cd}$$

$$A_{Epithermal} = 1.034 \ A^{Cd} - 0.0006 \ A^{bare} \ .$$

It was also necessary to correct for epithermal absorption in the monitor foils located near the edge of the HTLTR. Measured copper and gold cadmium ratios at the monitor location were used to evaluate these corrections. These corrections decreased the measured monitor foil activities by about 7% in thorium, 1% in copper, and 0.4% in plutonium. The relative thermal activation rates (in the central cell fuel to the monitor location) for the corrected thorium activation measurements agreed within experimental uncertainties with the corrected copper activation measurements. Since the thermal absorption cross sections of both thorium and copper are 1/v, this agreement between relative thermal activation rates tends to confirm the corrections made for epithermal absorption in the monitor foils.

Thermal cross sections at the monitor location were evaluated using a spectrum from a THERMOS[12] calculation of the HTLTR. The cross sections of the materials in the fissile fuel microspheres and the ThO_2 particles at the monitor location were calculated using an averaging routine CROSAV[12] which uses a collision probability routine together with the THERMOS fluxes and cross sections from the THERMOS BNW master library to calculate effective cross sections in the particle.

Measurement of Reactivities

Reactivity measurements were made by placing a sample in the void and measuring the change in reactor asymptotic period. The change in reactivity was then calculated using the inhour equation. A correction for the reactivity of the nitrogen in the void was calculated from the worth of copper in the void. Using the PuO_2-ThO_2 HTGR lattice as an example, this correction for the 7-1/2 x 7-1/2 x 24-inch void and the corrected reactivity worths for the various central cells, copper, and graphite, are summarized in Table B.1. The central cell worth, corrected for graphite end caps, is included in Table B.1. These reactivity worths include the N_2 in the pores of the graphite.

TABLE B.1. Reactivity Worth Measurements

	20°C, ¢	300°C, ¢	500°C, ¢	750°C, ¢	1000°C, ¢
N_2 Correction	-0.96	-0.49	-0.32	-0.22	-0.16
Standard 4 Block					
Central Cell (W/End Caps)	+13.57	+11.98	+11.33	+9.91	+7.29
(Without End Caps)	+11.90	+10.10	+9.27	+7.74	+5.05
Copper in Void (209.898 g)	-3.64	-3.40	-3.15	-2.90	-2.75
Graphite Carrier (2038 g)	+2.17	+2.44	+2.67	+2.83	+2.89

Additional measurements were made at room temperature in air. These measurements included a measurement of the copper worth on the carrier versus the copper worth in the void and the worth of an amount of graphite equivalent to the end cap region on the central cell. The effect of the carrier graphite was found to increase the worth per gram of copper on the carrier, relative to copper placed alone in the void, by (3.3 ± 0.8)%. This normalization was used to evaluate copper worths in the void at elevated temperatures from the measured copper worths on the carrier. The worth per gram of the dummy end cap graphite was (5 ± 2)% larger than the worth per gram of the

B.9

graphite carrier. Similarly, this normalization was used to evaluate the end cap worth at elevated temperatures from the measured graphite carrier worth.

The HTGR experiments utilized the remote sample changer for the HTLTR, shown in Figure 7. This device allowed samples to be preheated before insertion in the reactor and thus enables temperature transients during sample changes to be minimized. This resulted in a time saving during reactivity measurements and an improvement in accuracy. Errors have not been included in Table B.1, but typical errors might be ±0.02¢ at room temperature, ±0.04¢ at 300°C, 500°C, and 750°C, and ±0.07¢ at 1000°C. These errors are estimated from the consistency of the data and represent approximately one standard deviation. A second advantage of the remote sample changer was the elimination of the extension effect which created an uncertainty in earlier experiments.[7,21]

DISTRIBUTION

No. of
Copies

OFFSITE

12 DOE/Office of Scientific and
       Technical Information

    U.S. Department of Energy
      F-434/GTN
    Advanced Reactor Programs, NE-45
    Washington, D.C.   20545
    Attn: A. C. Millunzi

    U.S. Department of Energy
    Office of New Production Reactors
    613-104/FOR
    Washington, D.C.   20585.
    Attn: J. D. Nulton

    EG&G Idaho, Inc.
    P.O. Box 1625
    Idaho Falls, ID 83415
    Attn: R. K. McCardell

  7 Los Alamos National Laboratory
    P.O. Box 1663, MS K575
    Los Alamos, NM 87545
    Attn: G. E. Hansen
           J. E. Hanson
           W. L. Kirchner
           J. J. Malanify
           R. G. Palmer
           W. H. Reed
           J. L. Sapir

No. of
Copies

ONSITE

    DOE Richland Operations Office

       J. M. Hennig

  5 Westinghouse Hanford Company

       D. S. Dutt
       M. K. Korenko
       L. A. Lawrence
       R. P. Omberg
       R. W. Powell

 18 Pacific Northwest Laboratory

       W. J. Apley
       L. R. Dodd
       G. J. Konzek
       D. F. Newman (5)
       A. W. Prichard
       B. D. Shipp
       R. I. Smith
       H. H. Van Tuyl
       Publishing Coordination
       Technical Report Files (5)

DO NOT MICROFILM
THIS PAGE